Posttranslational modification of the RHO of plants protein RACB by phosphorylation and cross-kingdom conserved ubiquitination

Lukas Weiß[1], Lana Gaelings[1,2], Tina Reiner[1], Julia Mergner[3], Bernhard Kuster[3,4], Attila Fehér[5], Götz Hensel[6], Manfred Gahrtz[6], Jochen Kumlehn[6], Stefan Engelhardt[1], Ralph Hückelhoven[1]*

*Corresponding author; mail: hueckelhoven@tum.de

Affiliations:

[1]Chair of Phytopathology, Technical University of Munich (TUM), 85354 Freising, Germany

[2]Present address: [2]Chair of Brewing and Beverage Technology, Technical University of Munich (TUM), 85354 Freising, Germany

[3]Chair of Proteomics and Bioanalytics, Technical University of Munich (TUM), Freising, Germany

[4]Bavarian Biomolecular Mass Spectrometry Center (BayBioMS), TUM, Freising, Germany

[5]Chair of Plant Biology, University of Szeged, and Institute of Plant Biology, Biological Research Centre, Szeged, Hungary

[6]Institute of Plant Genetics and Crop Plant Research (IPK), Gatersleben

Abstract

Small RHO-type G-proteins act as signaling hubs and master regulators of polarity in eukaryotic cells. Their activity is tightly controlled, as defective RHO signaling leads to aberrant growth and developmental defects. Two major processes regulate G-protein activity: canonical shuttling between different nucleotide bound states and posttranslational modification (PTM), of which the latter can support or suppress RHO signaling, depending on the individual PTM. In plants, regulation of Rho of plants (ROPs) signaling activity has been shown to act through nucleotide exchange and GTP hydrolysis, as well as through lipid modification, but there is little data available on phosphorylation or ubiquitination of ROPs. Hence, we applied proteomic analyses to identify PTMs of the barley ROP RACB. We observed *in vitro* phosphorylation by barley ROP binding kinase 1 and *in vivo* ubiquitination of RACB. Comparative analyses of the newly identified RACB phosphosites and human RHO protein phosphosites revealed conservation of modified amino acid residues, but no overlap of actual phosphorylation patterns. However, the identified RACB ubiquitination site is conserved in all ROPs from *Hordeum vulgare*, *Arabidopsis thaliana* and *Oryza sativa* and in mammalian Rac1 and Rac3. Point mutation of this ubiquitination site leads to stabilization of RACB. Hence, this highly conserved lysine residue may regulate protein stability across different kingdoms.

Introduction

Small guanosine triphosphate-binding (G-) proteins are master regulators of developmental and immunity-related processes including membrane transport, nuclear protein trafficking, reactive oxygen species production and cytoskeleton organization in growth and immunity (Irani et al., 1997; Lin and Yang, 1997; Jones et al., 2002; Yang, 2008; Ebine et al., 2011; Akamatsu et al., 2013). In humans (*Homo sapiens*, *Hs*), small G-proteins are organized in the rat sarcoma (RAS) superfamily, comprised of the ARF, RAB, RAN, RAS and RHO families (Wennerberg et al., 2005), with the latter being further divided into Cdc42-like, Rho-like, RAC-like, RhoBTB and Rnd subfamilies (Lawson and Ridley, 2018). Plants possess ARF, RAB

43 and RAN family proteins, but only one type of small G-proteins from the RAS homologue
44 (RHO) family, so called Rho of plants (ROPs). Traditionally, they were also called plant RACs
45 (RAS-related C3 botulinum toxin substrate), due to their slightly higher similarity to metazoan
46 RACs than RHO proteins. ROPs can be further distinguished based on their C-terminal
47 hypervariable region and associated lipid modification. Type I ROPs can be reversibly
48 *S*-acylated and additionally contain a CaaX-box motif that is a target for constitutive cysteine
49 prenylation. Type II ROPs lack the CaaX-motif and are apparently constitutively *S*-acylated.
50 Those cysteine lipid modifications are essential for plasma membrane anchoring and
51 downstream signaling (Sorek et al., 2011; Yalovsky, 2015). Additionally, RHO proteins are
52 often called molecular switches, because they cycle between a guanosine diphosphate (GDP)-
53 bound "OFF" state and the signaling-competent guanosine triphosphate (GTP)-bound "ON"
54 state. This cycling itself is tightly controlled by specific proteins: guanosine nucleotide
55 exchange factors (GEFs) facilitate the GDP to GTP exchange, which leads to G-protein
56 activation. In turn, GTPase activating proteins (GAPs) target GTP-bound G-proteins and
57 stimulate their weak intrinsic GTPase activity, which results in GTP hydrolysis and turns the
58 G-proteins signaling incompetent (Berken and Wittinghofer, 2008). This nucleotide exchange
59 is accompanied by a conformational shift, which affects the interaction with other proteins
60 (Milburn et al., 1990; Berken, 2006). A third class of regulatory proteins, so-called guanine
61 nucleotide dissociation inhibitors (GDIs), targets mostly the GDP-bound state and recruits the
62 G-protein to the cytoplasm, blocking it from downstream signaling (Boulter and Garcia-Mata,
63 2010).

64 Lipidations are not the only posttranslational modifications (PTM) in RHO proteins. In animals,
65 both phosphorylation and ubiquitination are employed to control RHO signaling, thereby
66 enhancing or suppressing G-protein function in a case-dependent manner. The mammalian
67 RHO family member Rac1 for instance is phosphorylated at three amino acids and
68 ubiquitinated at two residues (reviewed in Abdrabou and Wang (2018)), whereas for
69 mammalian RhoA four phosphorylation sites and three ubiquitination sites have been identified
70 (Lang et al., 1996; Forget et al., 2002; Ellerbroek et al., 2003; Ozdamar et al., 2005; Rolli-

Derkinderen et al., 2005; Wei et al., 2013; Tang et al., 2014; Tong et al., 2016) (see S1 Fig for an overview of Rac1 and RhoA PTMs).

Compared to the mammalian field, knowledge about phosphorylation and ubiquitination in ROPs is limited. To date, *in vitro* phosphorylation of *Arabidopsis thaliana* (At) ROP4 and ROP6 by ROP binding protein kinase 1 (RBK1), a receptor-like cytoplasmic kinase (RLCK) of class VI_A, has been reported. RBK1 further interacts with Mitogen-activated protein kinase 1 (MPK1) of an auxin-responsive MPK cascade, and it has been suggested that regulation of ROP4 and ROP6 via phosphorylation might be important for auxin-dependent cell expansion (Enders et al., 2017). Furthermore, type II AtROP10 and AtROP11 are phosphorylated at S138, but no functional studies about these phosphosites have been conducted yet (Mergner et al., 2020). Introduction of a phosphomimetic mutation of the broadly conserved S74 in AtROP4 and *Medicago sativa* MsROP6 has been investigated. This S74E mutation did not alter GTPase activity, but blocked interaction with an upstream activating ROPGEF, weakened the binding to a downstream signaling kinase and stimulated less *in vitro* kinase activity (Fodor-Dunai et al., 2011). However, there is no reported evidence for *in vivo* phosphorylation of type I ROPs.

ROPs have been also investigated in the interaction between barley (*Hordeum vulgare, Hv*) and the powdery mildew fungus *Blumeria graminis* f.sp. *hordei* (*Bgh*). There it was shown that most barley ROPs can support the penetration success of *Bgh* (Schultheiss et al., 2002; Schultheiss et al., 2003; Pathuri et al., 2008; Hoefle et al., 2011). Among these barley ROPs, RACB is the best characterized ROP family member. Under physiological conditions, it is required for root hair outgrowth and stomatal subsidiary cell formation, and RACB and its interacting proteins further steer cytoskeleton organization (Engelhardt et al., 2019). During *Bgh* attack, RNA-interference (RNAi)-mediated knockdown of RACB decreased the penetration success of the fungus into barley epidermal cells, whereas overexpression of a constitutively activated RACB variant (CA, RACB-G15V, a GTPase mutant that cannot hydrolyse GTP) promoted susceptibility (Schultheiss et al., 2002; Schultheiss et al., 2003;

Pathuri et al., 2008; Hoefle et al., 2011). In contrast, transient overexpression of neither wildtype (WT) nor a dominant negative RACB form (DN, RACB-T20N, a mutant that can only bind GDP) increased barley susceptibility, indicating that the GTP-bound, signaling-active form of RACB supports fungal invasion into intact barley leaf epidermal cells.

Since RHO family proteins interact with several downstream executors to perform their signaling function, interaction partners of RACB were investigated with regard to barley susceptibility to *Bgh*. It was shown that two classes of scaffolding proteins, Interactor of Constitutively Active ROPs/ROP-interactive partners (ICRs/RIPs) and ROP-interactive and CRIB-motif containing proteins (RICs), associate with CA-RACB at the plasma membrane and enhance penetration success of *Bgh* into barley epidermal cells when transiently overexpressed (Schultheiss et al., 2008; Engelhardt et al., 2019; McCollum et al., 2020). In contrast, two other interactors of activated RACB support resistance to fungal penetration. Microtubule-Associated ROP GTPase Activating Protein 1 (MAGAP1) enhances resistance towards *Bgh* and likely negatively regulates RACB by supporting GTP hydrolysis (Hoefle et al., 2011). Barley RBK1 interacts with CA-RACB in yeast and *in planta*, and CA-RACB increases RBK1 kinase activity *in vitro*. RBK1 may be a RACB-regulated kinase, since co-expression of CA-RACB and RBK1 results in co-localization of both proteins at the plant plasma membrane via recruitment of the otherwise cytosolic RBK1. However, unlike RACB, transient knockdown of RBK1 results in increased disease susceptibility and reduced microtubule stability (Huesmann et al., 2012). S-phase kinase 1-associated protein-like (SKP1L), an interactor of RBK1, is also involved in resistance towards *Bgh* (Reiner et al., 2016). SKP1L is a predicted subunit of an SCF E3 ubiquitin ligase complex, which targets specific proteins for polyubiquitination and proteasomal degradation (Hua and Vierstra, 2011). In line with this predicted function, it was demonstrated that RBK1, SKP1L and the 26S proteasome negatively influence protein abundance of transiently overexpressed CA-RACB. These proteins hence presumably act in a negative feedback-loop involving phosphorylation and ubiquitination of RACB (Reiner et al., 2016).

In this study, we confirm that the kinase activity of RBK1 is substantially enhanced in the presence of CA-RACB, leading to strong autophosphorylation of RBK1 and transphosphorylation of CA-RACB *in vitro*. Phosphosite mapping revealed novel phosphorylated residues in RACB that were not previously described to be modified in other RHO family proteins. We further found that CA-RACB displays an ubiquitination-typical appearance of high molecular weight derivatives after immunoprecipitation. Mass spectrometry revealed that CA-RACB is ubiquitinated at K167. Mutational studies support that RACB K167 is involved in regulating protein stability, but otherwise did not interfere with RACB's ability to recruit interaction partners or influence susceptibility of barley to *Bgh*. However, data demonstrate *in planta* ROP ubiquitination at a residue that is conserved in mammalian Rac1, Rac3 and all other ROPs of barley, rice and Arabidopsis.

Results

CA-RACB is phosphorylated by RBK1 *in vitro*

Since previous research suggested that RACB might be negatively regulated through the protein kinase RBK1 and ubiquitination (Reiner et al., 2016), we aimed to discover putative posttranslational modifications in RACB. First, we investigated the potential of RACB to be phosphorylated by RBK1, because it was previously shown that constitutively activated (CA-) RACB interacts with RBK1 *in vivo* and enhances RBK1's kinase activity *in vitro* (Huesmann et al., 2012). Therefore, we carried out an *in vitro* radiolabeling kinase assay with recombinantly expressed and purified RBK1 and CA-RACB, both C-terminally His-tagged (Fig 1A). C-terminal tagging should prevent artificial phosphorylation events, as Dorjgotov et al. (2009) showed RBK1-like RLCK VI_A kinases phosphorylating the N-terminal His-tag and linker-region of *Medicago sativa Ms*ROP6, but not the ROP protein itself. Since RBK1 alone shows some constitutive kinase activity and autophosphorylation *in vitro* (Huesmann et al., 2012), we used low RBK1 protein amounts in this assay to be able to see stimulated kinase activity. Under these conditions, only weak autophosphorylation of RBK1 was visible. In the presence of CA-RACB, however, we observed stronger autophosphorylation of RBK1 and transphosphorylation of CA-RACB. No phosphorylation could be detected after incubation with a RBK1 kinase-dead mutant (KD, K245D) or in a water-control (see Fig 1B for RBK1 protein stability).

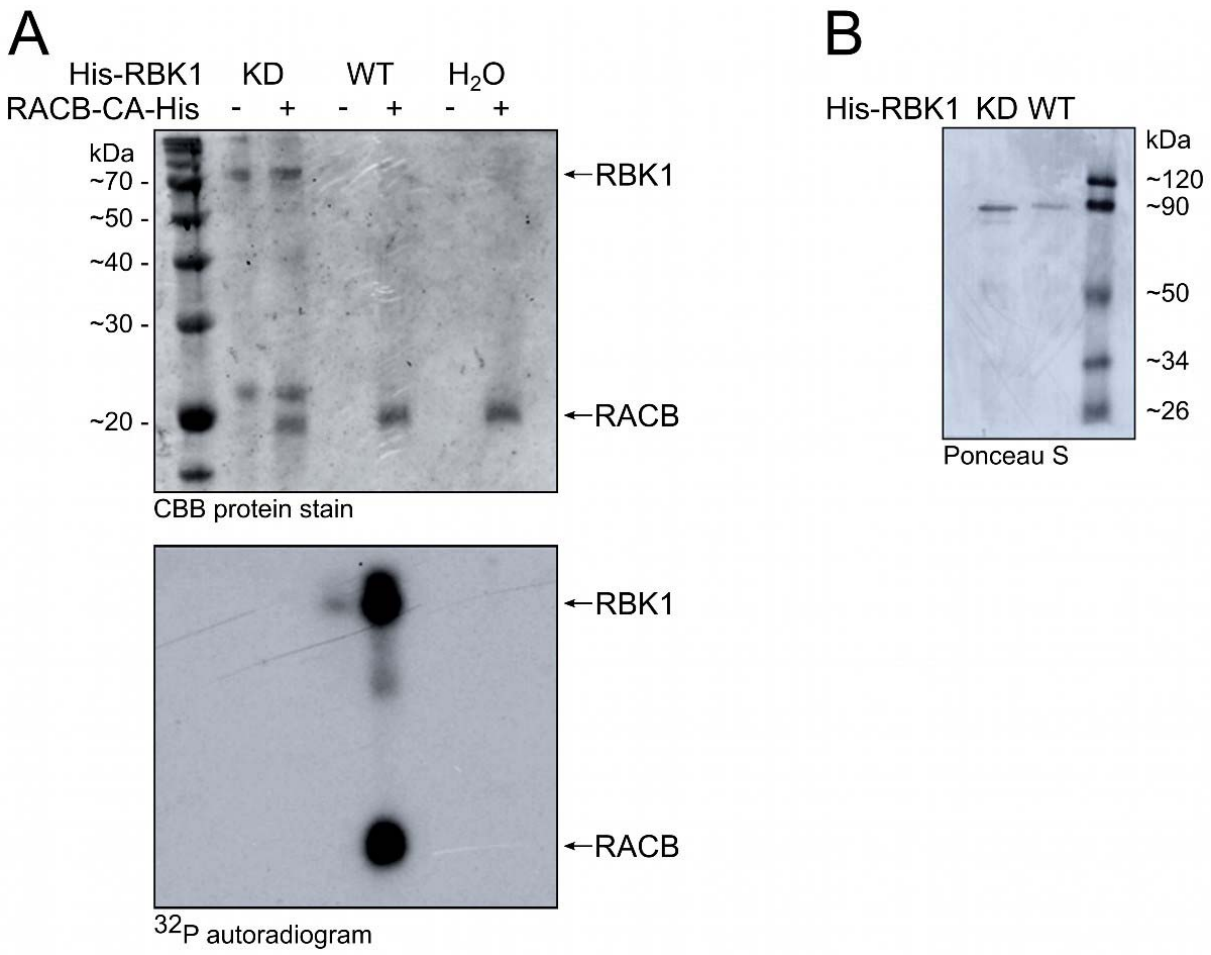

Fig 1. *In vitro* co-incubation of CA-RACB and RBK1 results in phosphorylation of both proteins.

(A) Low amounts of His-tagged RBK1 alone showed weak autophosphorylation *in vitro*. Kinase activity was enhanced by the presence of constitutively activated His-tagged CA-RACB, resulting in extensive phosphorylation of both proteins. Upper panel = protein loading control. Lower panel = autoradiogram showing ^{32}P-labelled, phosphorylated proteins. WT = wildtype RBK1; KD = kinase-dead RBK1 loss-of-function mutant (K245D); H_2O = no kinase control. Estimations of molecular weight are depicted in kilo Dalton (kDa) on the left.

(B) Ponceau S stain showing stability of purified WT and KD His-RBK1.

To eventually prove phosphorylation within the RACB protein sequence and to identify phosphosites in RACB, we conducted the *in vitro* kinase assay using RBK1 and unlabeled

ATP and detected *in vitro* phosphosites of CA-RACB via mass spectrometry after tryptic digestion (Fig 2A). This revealed high confidence CA-RACB peptides with phosphorylated residues at positions S97, T139, S159, S160 and T162. Since in the case of the neighboring serines S159 and S160 the localization of the phospho-modification could not be specifically assigned within the peptide sequence (S1 Table), both residues were treated as possible but alternative phosphosites. Using computational modelling of the RACB protein structure based on the protein models of GDP-bound *At*ROP4 and GTP-analog-bound *Hs*RAC1, we suggest that S97, T139 and T162 are surface-exposed in RACB, whereas this is less clear for S159 and S160 (Fig 2B).

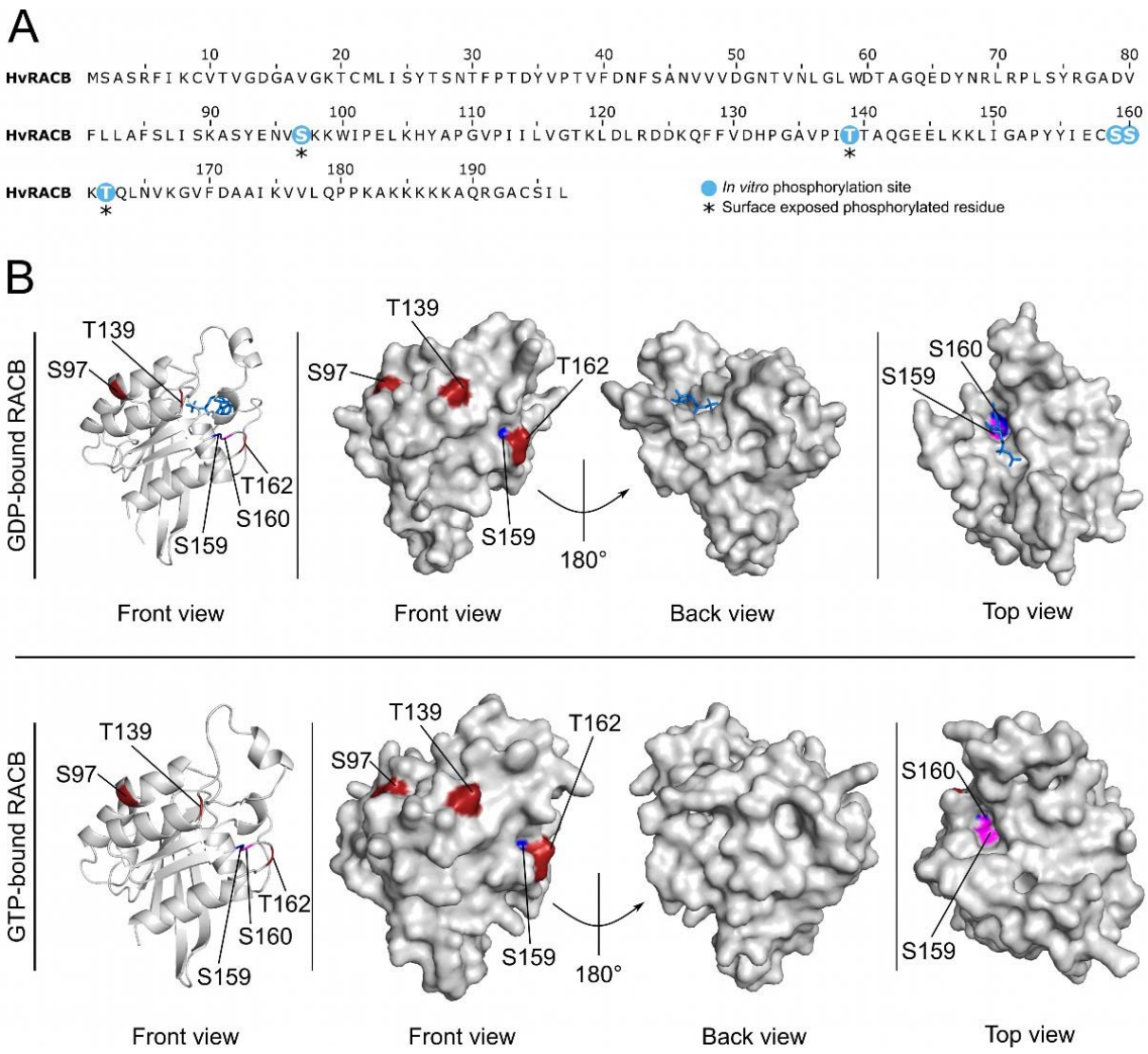

181 **Fig 2. Surface-exposure of CA-RACB *in vitro* phosphosites.**

182 **(A)** Phosphorylation sites of CA-RACB are shown in blue or, when phosphorylated and
183 predicted as surface-exposed, residues are additionally highlighted by asterisks. *In vitro*
184 phosphorylation sites of RACB were identified by mass spectrometry after *in vitro* co-
185 incubation of CA-RACB and RBK1.

186 **(B)** Upper panel: the model of GDP-bound WT RACB (amino acids 1-178 from 197 total) was
187 built with GDP-bound *At*ROP4 as template (PDB entry: 2NTY.1 (Thomas et al., 2007)). Lower
188 panel: GTP-bound WT RACB (amino acids 7-178 from 197 total) was modelled using *Hs*RAC1
189 associated with GNP (phosphoaminophosphonic acid-guanylate ester, a non-hydrolysable
190 GTP-analog) as template (PDB entry: 3TH5.1 (Krauthammer et al., 2012)). Phosphorylated
191 surface-exposed residues are highlighted in red, GDP as ligand in blue. Only S97, T139 and
192 T162 are surface-exposed, S159 (pink) and S160 (blue) are not clearly exposed to the surface.
193 Putative RACB folds were assembled by homology-modelling using SWISS-MODEL and
194 achieved GMQE (global model quality estimate) scores of 0.75 for GDP-RACB and 0.66 for
195 GTP-RACB, and QMEAN DisCo (qualitative model energy analysis with consensus-based
196 distance constraint) (Studer et al., 2020)) scores of 0.82 ± 0.07 and 0.80 ± 0.07, respectively.
197 Surface structure (front, back and top view) and cartoon (front view) illustrations were modelled
198 in PyMOL (Schrodinger, 2015).

199

200 Next, we tried to map *in vivo* phosphorylation sites for RACB. In order to obtain sufficient
201 amounts of protein, we generated transgenic barley lines overexpressing HA-tagged
202 CA-RACB, a cytosolic non-prenylated CA-RACB-ΔCSIL mutant (Schultheiss et al., 2003) or
203 the HA-tag alone. Initially, we generated 47 transgenic plants for HA-CA-RACB, 37 plants for
204 HA-RACB-ΔCSIL and 40 plants for HA alone. We propagated these lines and selected the
205 offspring using PCR, resistance against the selection marker hygromycin and Western blotting
206 (not shown). When we confirmed the expression of the HA-tagged RACB variants by Western
207 blot, only the free HA-peptide could not be detected, most likely because of its small size (Fig

208 3A). Since CA-RACB is a susceptibility factor in the barley-*Bgh* interaction (Schultheiss et al.,
209 2002; Schultheiss et al., 2003; Pathuri et al., 2008; Hoefle et al., 2011), we also scored the
210 penetration efficiency of *Bgh* in leaf epidermal cells of all three transgenic lines to rule out any
211 artificial effects of the HA-tag on the susceptibility function of RACB during the barley-*Bgh*
212 interaction. Upon infection with *Bgh*, plants overexpressing full-length HA-CA-RACB displayed
213 increased disease susceptibility compared to the free HA-control similar as shown before for
214 untagged CA-RACB (Pathuri et al., 2008), whereas the HA-CA-RACB-ΔCSIL overexpressing
215 plants did not show an increased disease phenotype (Fig 3B). This suggests that HA-tagged
216 CA-RACB is functional in support of fungal penetration.

217

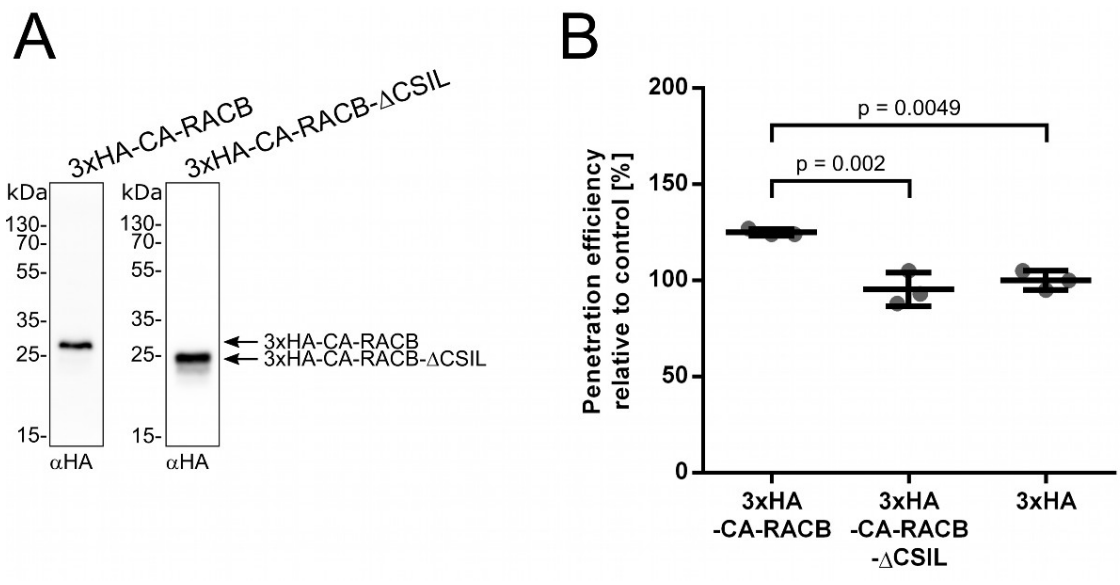

218

219 **Fig 3. Transgenic barley plants overexpressing HA-tagged CA-RACB show increased**
220 ***Bgh* susceptibility.**

221 **(A)** Both HA-tagged full-length CA-RACB and CA-RACB-ΔCSIL are stably expressed in
222 transgenic barley. Eluate fractions of anti-HA immunoprecipitations were analyzed by anti-HA
223 Western blotting. Plant material belonged to pools of transgenic lines BG657 E3 and E4 for
224 *3xHA-CA-RACB* and BG658 E4 and E9 for *3xHA-CA-RACB*-ΔCSIL.

225 **(B)** Leaf epidermal cells of transgenic plants expressing full-length HA-tagged CA-RACB were
226 more susceptible towards penetration by *Bgh*, while plants expressing the truncated CA-
227 RACB-ΔCSIL mutant show the same level of susceptibility as the HA-control. For each
228 construct, three plants of one transgenic line were tested. Lines were BG657 E4 for 3x*HA*-CA-
229 *RACB*, BG658 E4 for 3x*HA*-CA-*RACB*-ΔCSIL and BG659 E2 for 3x*HA*. Each datapoint
230 corresponds to one plant with about 100 interaction sites scored, and means with standard
231 deviation are shown. Statistical significances were determined using a One-way ANOVA with
232 Tukey's HSD.

233

234 To find *in vivo* phosphorylation sites of RACB, we initially isolated leaf mesophyll protoplasts
235 from HA-CA-RACB overexpressing plants and, to eliminate any negative impact on RACB
236 stability caused by phosphorylation as previously hypothesized (Reiner et al., 2016), we
237 treated them with the proteasome inhibitor MG132. We extracted total proteins from these
238 protoplasts and enriched HA-tagged CA-RACB using immunoprecipitation. Following tryptic
239 digestion, we selected for phosphorylated peptides using Immobilized Metal Affinity
240 Chromatography (IMAC). Peptides and posttranslational modifications were identified via
241 mass spectrometry, but potential HA-CA-RACB phosphosites eluded our detection (not
242 shown). Next, before MG132 treatment, we co-overexpressed GFP-tagged RBK1 in mesophyll
243 protoplasts prepared from transgenic HA-CA-RACB overexpressing and control plants, and
244 selectively skipped immunoprecipitation or IMAC (S2A Fig). This attempt also did not lead to
245 the identification of *in vivo* RACB phosphopeptides, although more than 2,000 barley proteins
246 were found to phosphorylated in those samples (S2 Table). In a third approach, we tried to
247 map RACB phosphorylation after transient co-overexpression of GFP-RBK1 and proteasome
248 inhibition by MG132 in transgenic HA-CA-RACB overexpressing barley mesophyll protoplasts.
249 From this, we extracted proteins, performed a tryptic digest and enriched phosphopeptides via
250 IMAC. These samples were subsequently decomplexed by high pH reversed-phase
251 fractionation to increase the discovery rate of peptides during mass spectrometry. This

252 identified more than 5,000 phosphopeptides from diverse barley proteins (S3 Table), thus
253 providing a valuable resource for the barley research community. For instance, data show in
254 vivo phosphorylation sites of ROP signaling components such as three different barley
255 ROPGAPs (S4 Table). Because our experimental design included *in vivo* expression of
256 combined or single GFP-tagged RBK1 and HA-CA-RACB (S2B Fig), some of the mapped
257 barley phosphosites might be CA-RACB- and/or RBK1-dependent, but this would need further
258 validation. Despite the high amount of identified phosphopeptides, no *in vivo* phosphopeptides
259 of HA-CA-RACB were recovered.

260 Although we primarily aimed at identifying phosphopeptides of RACB, our datasets showed
261 phosphosites for RBK1 (Fig 4). In the *in vitro* kinase assay, we found RBK1 to be
262 phosphorylated at positions S26, S30, S98, S100, S107, T110, S155, T170 and S436. In the
263 two experiments involving *in vivo* co-overexpression of CA-RACB and RBK1 (S2A Fig and Fig
264 4C), we found RBK1 phosphosites at positions S26, S30, S107, S113, S160, T170, S189,
265 S197, S518, T521 and S26, S30, S100, S107, S113, S114, S216, T525, respectively.
266 Overlapping sites from *in vitro* and at least one *in vivo* experiment are therefore S26, S30,
267 S100, S107 and T170.

268

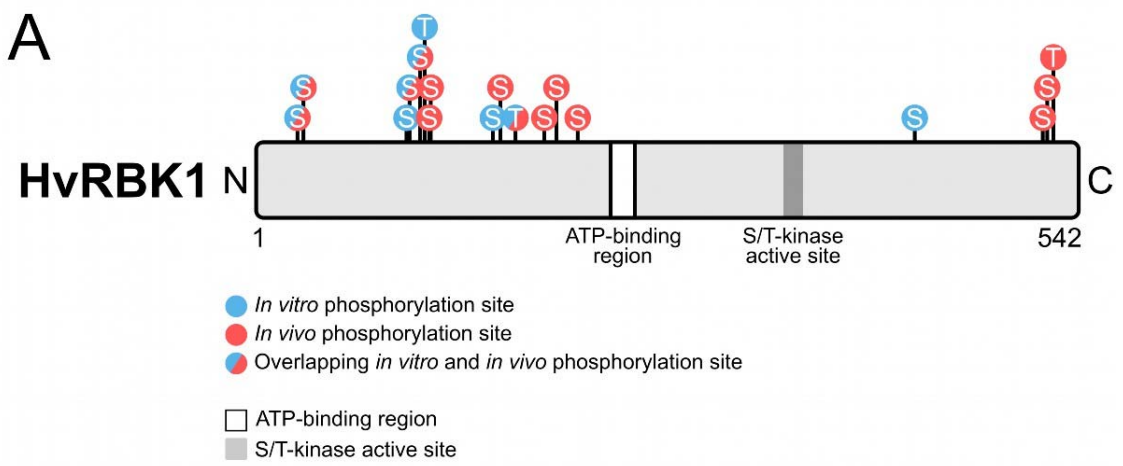

B

In vitro sites	*In vivo* sites experiment 1	*In vivo* sites experiment 2
S26	S26	S26
S30	S30	S30
S98	-	-
S100	-	S100
S107	S107	S107
T110	-	-
-	S113	S113
-	-	S114
S155	-	-
-	S160	-
T170	T170	-
-	S189	-
-	S197	-
-	-	S216
S436	-	-
-	S518	-
-	S521	-
-	-	T525

Fig 4. Comparison between *in vitro* and *in vivo* RBK1 phosphosites.

(A) Schematic illustration of the barley RBK1 sequence with marked *in vitro* (blue) and *in vivo* (red) phosphosites. Residues phosphorylated under both conditions are shown with both colors. *In vitro* phosphorylated amino acids were identified in an *in vitro* kinase assay, in which His-tagged RBK1 and His-tagged CA-RACB were co-incubated. *In vivo* phosphosites were found in transgenic HA-CA-RACB overexpressing mesophyll protoplasts in the presence of transiently co-overexpressed GFP-tagged RBK1 and the proteasome-inhibitor MG132. Phosphopeptides were enriched from total protein extracts of protoplast lysates using IMAC (experiment 1) and additionally decomplexed by high pH reversed-phase fractionation (experiment 2). All *in vitro* and *in vivo* phosphosites were identified by mass spectrometry.

(B) List of RBK1 phosphosites from all *in vitro* and *in vivo* experiments.

282 # CA-RACB is ubiquitinated *in vivo*

283 Previously, we found that the protein abundance of CA-RACB is negatively influenced by
284 RBK1, SKP1L and a proteasome (Reiner et al., 2016). This prompted us to investigate
285 potential *in vivo* CA-RACB ubiquitination. We used MG132 for proteasome inhibition in first
286 leaves of transgenic barley overexpressing HA-tagged CA-RACB. This led to detection of
287 HA-CA-RACB and higher molecular weight derivatives on Western blots after
288 αHA-immunoprecipitation and detection via anti-HA antibodies (Fig 5A). To determine whether
289 this band pattern is MG132 dependent, we repeated this experiment with a DMSO control and
290 found a similar laddering pattern in the control (S3 Fig). As this laddering is usually a
291 characteristic indicator for ubiquitination of a target protein (Gohre et al., 2008; Lu et al., 2011),
292 we attempted to map the residue(s) at which HA-CA-RACB might be ubiquitinated. We first
293 conducted a global mass spectrometry analysis, in which we specifically looked for branched
294 amino acid sequences that derive from ubiquitinated lysine residues after tryptic digest (S2C
295 Fig). Interestingly, we found a peptide containing RACB K167 carrying a mass shift equal to
296 2 glycine molecules (Fig 5B). This mass shift indicates that K167 is indeed ubiquitinated, as
297 two glycine residues typically remain at ubiquitinated lysine residues (glyglycylation), whereas
298 the rest of the ubiquitin moiety is cleaved by trypsin during sample digestion (Peng et al., 2003).
299 Evidence for RACB ubiquitination was subsequently substantiated in a targeted parallel
300 reaction monitoring (PRM) approach. Comparison with other ROPs from barley, rice and
301 Arabidopsis showed that RACB K167 is a highly conserved residue in ROPs (Fig 6 and S4
302 Fig).

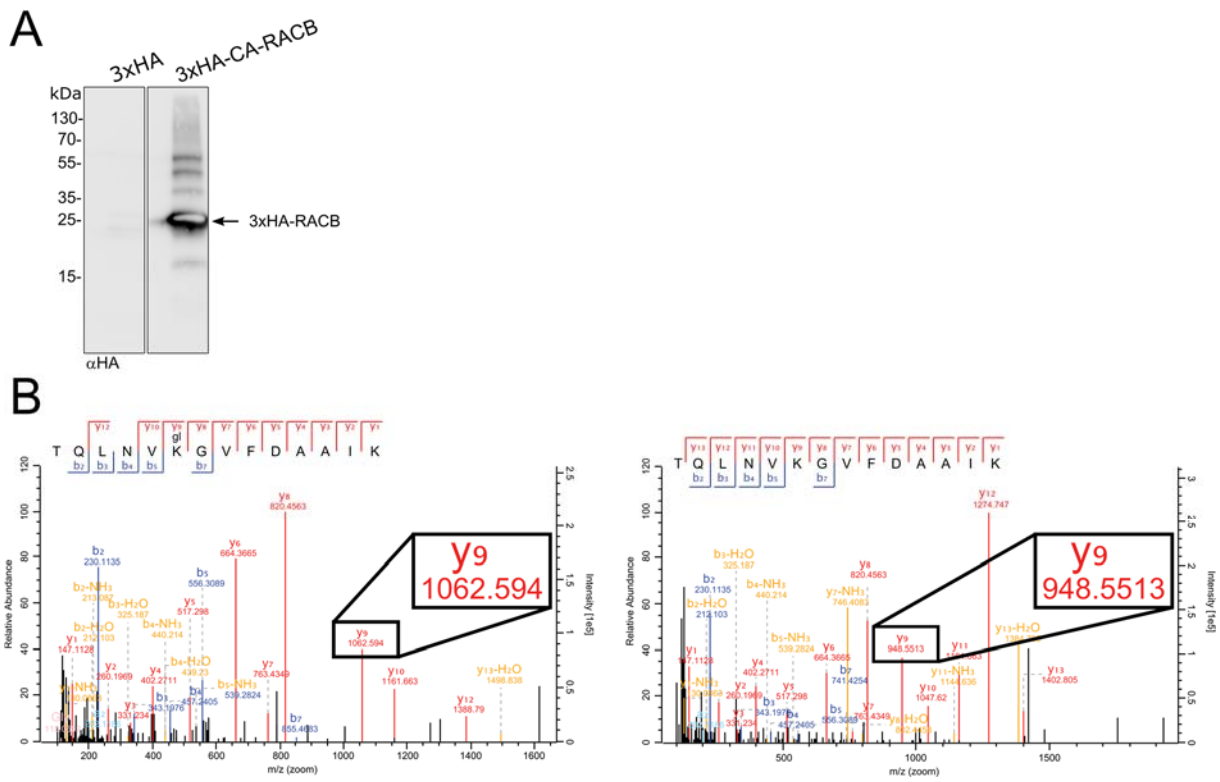

Fig 5. Constitutively activated RACB is ubiquitinated *in vivo*.

(A) HA-tagged CA-RACB and higher molecular weight bands were detected in an αHA-Western blot after MG132 treatment and αHA-immunoprecipitation from whole barley leaves stably expressing 3xHA or 3xHA-CA-RACB (Fig S2B). Plant material was pooled from transgenic lines BG657 E3 and E4 for 3xHA-CA-RACB and BG659 E2 and E3 for 3xHA.

(B) Ubiquitination of CA-RACB at K167 was identified by mass spectrometry in a workflow described in S2B Fig. The left graph shows spectra of the recovered ubiquitinated peptide, while the right graph shows the corresponding unmodified peptide. The black box illustrates one example of such a size difference: fragment "y9" was recovered with two different masses. The difference corresponds to that of 2 glycines, which is typical after a tryptic digest of ubiquitinated proteins (Peng et al., 2003). Example: $y9_{modified}$ (1062.59 m/z) – $y9_{unmodified}$ (948.55 m/z) = 114.04 m/z = 2 * glycine (57.02 m/z).

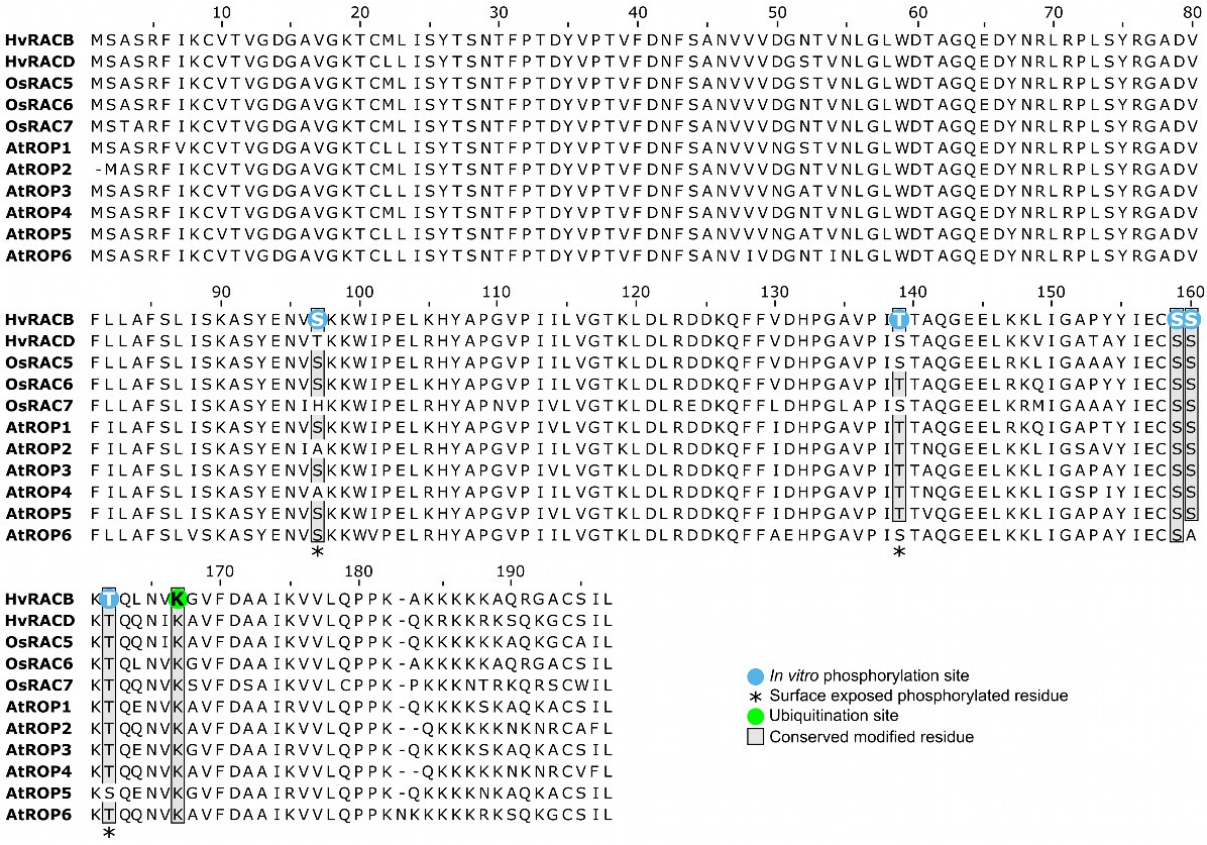

Fig 6. Alignment of type I ROPs from barley (*Hordeum vulgare*, *Hv*), rice (*Oryza sativa, Os*) and *Arabidopsis thaliana* (*At*).

The ubiquitinated lysine residue in barley RACB (K167, green) is conserved across all type I ROPs from the three species (shaded box). *In vitro* phosphosites of RACB (blue) are conserved among some type I ROPs (shaded box). Surface-exposed phosphosites are highlighted with asterisks.

RACB K167 regulates protein stability

Next, we wanted to know if RACB K167 plays a role in regulating protein stability. For this, we generated non-ubiquitinatable K167R mutants of the different RACB activity-variants (WT, CA, DN [dominant negative RACB-T20N (Schultheiss et al., 2003)]). We substituted lysine with arginine, because both amino acids are positively charged and structurally similar, but arginine is not recognized as an ubiquitin acceptor site. In order to assess if K167 influences protein

332 stability in barley epidermal cells, we fused GFP to the N-terminus of RACB and compared the
333 fluorescence levels of regular GFP-WT/CA/DN-RACB with those of their corresponding K167R
334 mutants via confocal microscopy after biolistic transformation (Fig 7). Since fluorescence levels
335 inherently vary between single transiently transformed cells, we co-expressed free mCherry
336 as a normalizer in all experiments and used the calculated ratio of GFP to mCherry
337 fluorescence for comparisons. Thereby, we measured that the K167R mutants of GFP-CA-
338 and GFP-DN-RACB showed stronger fluorescence signals than their original K167
339 counterparts, while the GFP-WT-RACB(-K167R) fluorescence levels displayed no difference.
340 Comparison of total protein abundance between RACB variants was not feasible, because
341 laser excitation levels had to be adjusted for imaging of WT/CA/DN-RACB.

342

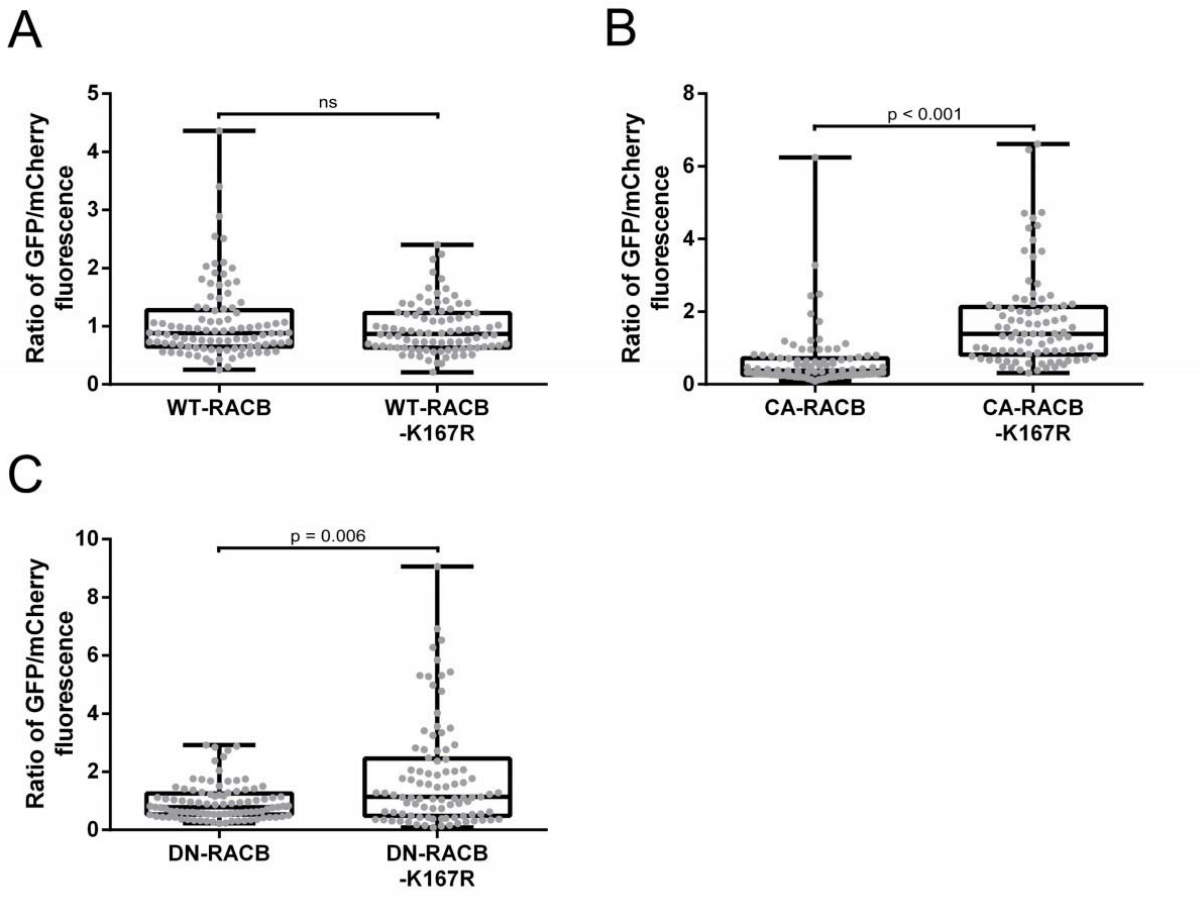

343

344 **Fig 7. Quantification of GFP-RACB(-K167R) fluorescence intensities.**

345 GFP-tagged RACB-variants (WT **(A)**, CA **(B)** and DN **(C)**) and their corresponding non-
346 ubiquitinatable K167R mutants were transiently expressed in single barley epidermal cells via
347 particle bombardment. Free mCherry was co-expressed in all experiments as a normalizer.
348 Mean pixel fluorescence intensities for GFP and mCherry were measured using a confocal
349 laser-scanning microscope. For comparison, ratios of fluorescence were calculated by dividing
350 the measured fluorescence signal of GFP-RACB by that of free mCherry in each individual
351 cell. In case of GFP-CA- and GFP-DN-RACB, the K167R mutants displayed higher
352 fluorescence levels than their non-mutated K167 counterparts, whereas GFP-WT-
353 RACB(-K167R) fluorescence levels were similar. Each datapoint represents one transformed
354 cell. All datapoints were collected over three biological replicates. Laser excitation levels were
355 different for all three RACB activity variants, but kept identical for regular and K167R RACB
356 forms. Statistical analysis was performed with Wilcoxon rank-sum tests with continuity
357 correction against a p-value of 0.05.

358

359 To confirm that the RACB-K167R mutants are properly folded proteins and signaling
360 competent, we tested if they are on one hand able to recruit downstream interactors to the
361 plasma membrane and on the other hand influence the susceptibility of barley in favor of *Bgh*.
362 We exclusively used CA-RACB in these experiments, since only this form of RACB was shown
363 to govern signaling processes (Schultheiss et al., 2003; Pathuri et al., 2008; Schultheiss et al.,
364 2008). In order to check if CA-RACB-K167R is promoting susceptibility to fungal cell entry in
365 the barley-*Bgh*-interaction, we transiently overexpressed untagged CA-RACB(-K167R) or an
366 empty vector control in barley epidermal cells before challenge inoculation with *Bgh* (Fig 8). At
367 40 hpi, we recorded a 39.4% or 34.6% increased susceptibility towards fungal penetration in
368 cells overexpressing CA-RACB or CA-RACB-K167R, when compared to the control. Hence,
369 we detected no difference in support of fungal penetration efficiency between CA-RACB and
370 CA-RACB-K167R. For testing possible recruitment of a known RACB downstream interactor,
371 we chose RIC171 because it was shown before to enrich at the cell periphery or plasma

membrane when CA-RACB was co-expressed (Schultheiss et al., 2008). We used mCherry-RIC171 and GFP-CA-RACB(-K167R) fusion proteins for confocal microscopy in transiently transformed barley epidermal cells (Fig 9). Free CFP was co-expressed in all combinations as a marker for cytoplasmic and nuclear fluorescence. We observed that mCherry-RIC171 was strongly recruited towards the cell periphery in the presence of both GFP-CA-RACB and GFP-CA-RACB-K167R. No obvious recruitment of mCherry-RIC171 was detectable when free GFP was co-overexpressed and mCherry-RIC171 localized to the cytoplasm and nucleoplasm in this case.

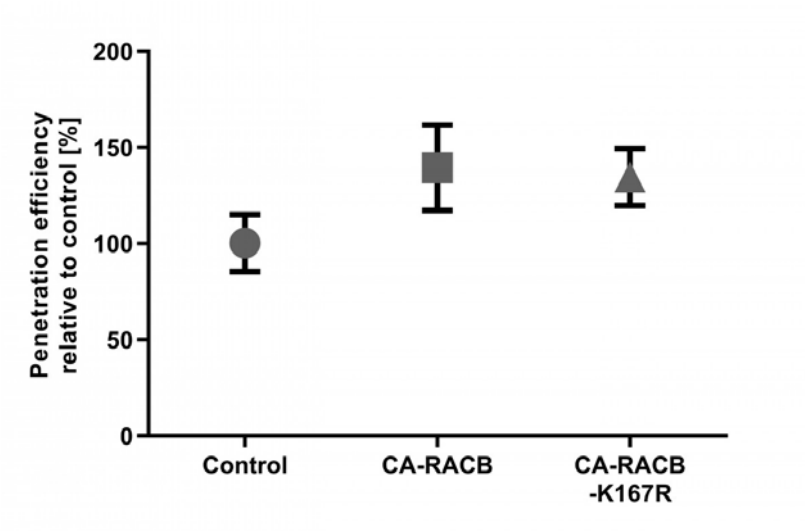

Fig 8 CA-RACB-K167R, similar to CA-RACB, increases barley susceptibility towards *Bgh*.

Transient overexpression of untagged CA-RACB and CA-RACB-K167R in barley epidermal cells resulted in increased susceptibility towards *Bgh* when compared to the empty vector control. Transient transformation was achieved using particle bombardment. Fungal susceptibility was assessed 40 hpi. Mean *Bgh* penetration efficiency and standard error of the mean of 5 fully independent biological replicates are shown. Each datapoint represents one biological replicate, in which the penetration efficiency of *Bgh* was calculated using a minimum

390 of 50 individual cells. Only single transformed barley epidermal cells were considered for
391 analysis.

392

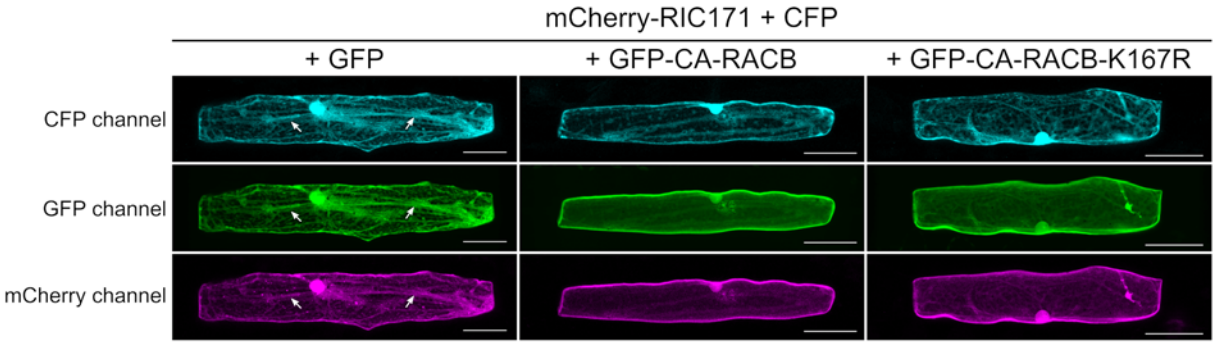

393

394 **Fig 9. Recruitment of mCherry-RIC171 by GFP-CA-RACB-K167R.**

395 Localization of the mCherry-tagged RACB-interactor RIC171 (Schultheiss et al., 2008) was
396 imaged in the presence of either free GFP, GFP-CA-RACB or GFP-CA-RACB-K167R. Free
397 CFP was co-expressed in all cells as a marker for cytosolic and nuclear localization. All
398 proteins were expressed transiently in barley epidermal cells via particle bombardment. In the
399 absence of GFP-CA-RACB, mCherry-RIC171 fluorescence co-localized with GFP and CFP in
400 the cytoplasm and nucleus (left panels, white arrows indicate cytosolic transvacuolar strands).
401 When GFP-CA-RACB (center panels) or GFP-RACB-CA-K167R (right panels) were
402 co-expressed, mCherry-RIC171 re-localized towards the periphery of the cell and showed only
403 background fluorescence in the cytoplasm and nucleus. Representative images of three
404 independent experiments are shown. In each experiment 15 cells per combination were
405 imaged. Images display Z-stack maximum intensity projections of slices with 2 µm step
406 increments. Brightness of the images was enhanced by 20% post-scanning for better visibility.
407 The white scale bar in the bottom right corner of each panel represents 50 µm.

408 # Discussion

409 The function of RHO family proteins as signaling hubs and master regulators of cell polarity
410 must be tightly controlled. Posttranslational modifications of RHO proteins, which enhance or
411 suppress RHO protein activity, such as lipid modifications, phosphorylation and ubiquitination,
412 have been well described in recent years (Abdrabou and Wang, 2018). Other PTMs including
413 glycosylation and adenylylation have been predominantly demonstrated to be caused by
414 virulence effectors from pathogenic organisms that target RHO family proteins of their hosts
415 (Worby et al., 2009; Jank et al., 2013).

416 The regulation of ROP activity in plants by GEFs and GAPs has been well documented and
417 occurs via their influence on the nucleotide binding state of the G-protein (Wu et al., 2000;
418 Berken et al., 2005; Klahre and Kost, 2006; Hoefle et al., 2011; Akamatsu et al., 2013).
419 However, for plants there is little data available on ROP activity regulation via posttranslational
420 modifications beyond prenylation and *S*-acylation (Yalovsky, 2015). In this study, we show *in*
421 *vivo* ubiquitination of a plant RHO protein, and our data also suggest a biological role for this
422 PTM. Using transgenic barley plants overexpressing a CA-RACB variant, we identified higher
423 molecular weight RACB derivatives on a Western blot, reminiscent of a typical ubiquitination
424 pattern as described for e.g. the plant pattern-recognition receptor flagellin sensing 2 (FLS2)
425 (Gohre et al., 2008; Lu et al., 2011). Mass spectrometry analysis evidenced RACB K167 as an
426 ubiquitin acceptor site, which is fully conserved across all ROPs of barley, rice and Arabidopsis
427 (Fig 6 and S4 Fig). The presence of this particular lysine even in mammalian Rac1 and Rac3
428 (Zhao et al., 2013; Dong et al., 2014) suggests a highly conserved ubiquitination motif across
429 kingdoms. Conservation of two other ubiquitination sites from mammalian RHO proteins in
430 RACB suggests that general regulatory mechanisms for small G-proteins could be conserved
431 between plants and animals. Albeit we couldn't evidence RACB K8 and K148 being
432 ubiquitinated in our experimental setup, the corresponding lysines in RhoA and Rac1 are
433 targeted for ubiquitination (S1 Fig), which influences actin cytoskeleton dynamics and
434 associated cellular processes, such as cell motility, in mammalian cells (Wang et al., 2003;
435 Ozdamar et al., 2005; Torrino et al., 2011; Oberoi et al., 2012; Castillo-Lluva et al., 2013).
436 Nonetheless, it is not yet known whether and under which conditions a modification of these

437 conserved sites might occur in ROPs. Regarding RACB, an association with protein
438 degradation was supported by mutating specifically RACB-K167 to a non-ubiquitinatable
439 arginine in various GFP-tagged RACB activity-variants (WT, CA, DN). CA-RACB-K167R was
440 drastically more abundant than CA-RACB in barley epidermal cells, whereas this was less
441 pronounced, but consistent for DN-RACB-K167R. Interestingly, the abundance of WT-RACB
442 was not significantly influenced by the K167R mutation, which might be explained by the fact
443 that wildtype RACB can still shuttle between GEF/GAP-mediated ROP activation and
444 deactivation, whereas ubiquitination might be a slower process that predominantly takes place
445 if RACB is arrested in a nucleotide bound form. Alternatively, efficient deubiquitination might
446 be restricted to regulated WT-RACB. Generally, activated GTP-RACB could be ubiquitinated
447 as an additional means of the plant cell to terminate active G-protein signaling besides
448 inactivation via hydrolysis of GTP. This seems reasonable and could be conserved across
449 kingdoms, as a similar mechanism has been shown for mammalian GTP-Rac1, which is
450 ubiquitinated at the corresponding K166 to remove it from signaling in cell motility (Zhao et al.,
451 2013). On the other hand, the purpose of ubiquitination of signaling incompetent DN-RACB
452 could be a simple disposal mechanism.

453 The presence or absence of the protein stability-regulating lysine doesn't appear to impinge
454 on RACB-mediated downstream signaling. Both ubiquitinatable and non-ubiquitinatable
455 CA-RACB could recruit the interaction partner RIC171 to the cell periphery, which was
456 described before (Schultheiss et al., 2008). Additionally, overexpression of the higher
457 abundant CA-RACB-K167R showed the same increase in barley susceptibility towards
458 penetration by *Bgh* as CA-RACB (Schultheiss et al., 2003; Schultheiss et al., 2008). Hence,
459 the sheer abundance of activated RACB might not be limiting for fungal penetration success
460 in a situation in which CA-RACB is overexpressed. However, ubiquitination could have an
461 impact on RACB's ability to interact with other proteins. For instance, non-ubiquitinated K167
462 is presumably bound by PRONE-GEFs and CRIB-domain-containing proteins, since it is in
463 both cases part of the respective binding interface (see S5 Fig, (Abdul-Manan et al., 1999;
464 Thomas et al., 2007; Schaefer et al., 2011)). Ubiquitination of K167 could hence sterically block

465 these interfaces and therefore hinder activation of RACB by PRONE-GEFs and interaction
466 with downstream CRIB-containing executors. In both scenarios, RACB signaling would be
467 effectively inhibited. In turn, it is likely that interaction of activated RACB with CRIB-domain-
468 containing executors, such as RIC proteins (Schultheiss et al., 2008; Engelhardt et al., 2019),
469 would mask the ubiquitination site. This could not only lead to increased protein stability, but
470 also secure RACB's signaling activity during crucial processes. In any case, RACB's upstream
471 or downstream interactors may have the potential to interfere with ubiquitination of RACB and
472 hence proteasomal degradation, but this remains to be tested in the future.

473 This ubiquitin-dependent regulation of RACB activity could also involve RBK1 and SKP1-like,
474 since RNAi-mediated knock-down of both proteins was shown to have a similar effect on RACB
475 abundance (Reiner et al., 2016). We previously hypothesized that RACB is regulated similarly
476 to mammalian Rac1. Phosphorylation of Rac1 S71 by AKT leads to SCF^{FBXL19}-mediated
477 ubiquitination at Rac1 K166 and subsequent proteasomal degradation, which blocks Rac1
478 from signaling (Kwon et al., 2000; Chang et al., 2011; Zhao et al., 2013). We speculated that
479 activated RACB might be phosphorylated by RBK1 and then targeted for ubiquitination and
480 degradation by an SCF-complex containing SKP1L (Huesmann et al., 2012; Reiner et al.,
481 2016). While we did find ubiquitination at RACB K167 (which corresponds to Rac1 K166, S1
482 Fig), we did not identify RACB S74 as a phosphorylation site although the motif was covered
483 in our MS data set. One potential reason for this might be that RBK1 belongs to RLCK class
484 VI_A (Jurca et al., 2008; Huesmann et al., 2012; Reiner et al., 2015), while AKT belongs to the
485 AGC kinases (Rademacher and Offringa, 2012). Interestingly, ROPs and AGCs also work
486 together in polar cell development. For instance, the AGCVIII kinase D6PK binds to specific
487 membrane lipids and cooperates with RACB-like type I *At*ROP2/*At*ROP6 to form root hairs
488 (Stanislas et al., 2015). Thus far, phosphorylation of ROPs during interaction with AGC kinases
489 has not been described, but it remains possible that AGC kinases phosphorylate ROPs, with
490 S74 being one of the potential targets.

491 In Arabidopsis and barley, ROPs and RBK1 or related RLCK VI_A-class kinases have partially
492 opposing biological functions. In previous studies, we have shown that gene silencing of barley
493 *RBK1* provoked the opposite disease phenotype as *RACB* and supports RACB protein
494 abundance (Huesmann et al., 2012; Reiner et al., 2016). In Arabidopsis, the ROP-activated
495 RBK1-homolog RLCK VI_A3 is similarly involved in pathogen resistance rather than
496 susceptibility (Reiner et al., 2015). Enders and co-workers could show that *rbk1* knock-out
497 plants displayed hypersensitivity towards auxin, while *atrop4* and *atrop6* mutants were
498 defective in auxin sensing. Furthermore, they suggested that *At*ROP4 and *At*ROP6 might be
499 direct phosphorylation targets of *At*RBK1 (synonym: RLCK VI_A4). They hypothesized that
500 *At*RBK1-mediated phosphorylation negatively influences the activity of both ROPs (Enders et
501 al., 2017). However, this remains to be shown, since phosphorylation was investigated *in vitro*
502 and no phosphosites were mapped in this study. Nevertheless, this suggests a perhaps
503 general mechanism, in which ROPs are negatively regulated by phosphorylation through
504 RLCK VI_A members in distinct signaling branches. However, we would like to stress that *in*
505 *vivo* phosphorylation of RACB by RBK1 could neither be proved nor disproved in this study.

506 The *in vitro* phosphosites S97, T139 and T162, which we identified in RACB, are predicted to
507 be surface-exposed and therefore could theoretically be targets for RBK1-dependent
508 phosphorylation of RACB *in vivo* (Fig 2). This is less clear for S159 and S160. Nevertheless,
509 one can speculate that these serine residues could become accessible *in vivo* after other
510 posttranslational modifications of RACB, which cause a conformational shift. Alternatively,
511 these sites become more exposed during interaction with RBK1. The positions of the
512 phosphosites within RACB suggest that the modification of particularly S159, S160 and T162
513 could interfere with RACB lipidation and nucleotide cycling, since these residues are next to
514 the putative *S*-acylation site C158 and the nucleotide binding pocket (Fig 2 and S1 Fig; (Sorek
515 et al., 2010; Sorek et al., 2017)). Furthermore, *in vivo* phosphorylation of all five residues could
516 affect RACB activation, as they are part of or in direct proximity of a conserved PRONE-GEF
517 binding interface (see S5 Fig, (Sørmo et al., 2006; Thomas et al., 2007; Fricke and Berken,
518 2009)). However, this remains a speculation at this point.

519 All five in *vitro* phosphorylated residues in RACB are partially conserved in other type I and
520 type II ROPs, indicating that these sites might be common targets for phosphorylation. The
521 only evidenced *in vivo* ROP phosphosite, S138 from *At*ROP10 and *At*ROP11 (S4 Fig; (Mergner
522 et al., 2020)), is not conserved in RACB, which indicates that this might be a type II ROP-
523 specific modification site. In any case, introducing point mutations at these sites could help
524 answering which role they play in regulating ROP function.

525 Comparison of RACB phosphosites with those of mammalian Rac1 and RhoA revealed that
526 there is no overlap between mapped animal and plant phosphosites, although several modified
527 residues are conserved across kingdoms (S1 Fig). Thus, it is well possible that RACB is also
528 phosphorylated at Y67, S74 and S89 by other kinases. Still, conservation of these amino acids
529 suggests that RACB could be regulated in a similar fashion as mammalian RHO family
530 proteins. Interestingly, phosphorylation of these residues in mammalian RHO proteins directly
531 and indirectly regulates actin cytoskeleton dynamics (Chang et al., 2011; Zhao et al., 2013;
532 Tong et al., 2016), a process also influenced by RACB in barley (Opalski et al., 2005).
533 Therefore, it remains conceivable that phosphorylation of these conserved sites may be
534 important for ROP regulation during plant cytoskeleton rearrangement.

535 Using stable transgenic plants, our data further support that posttranslational prenylation may
536 be important for the signaling ability of RACB. Full-length CA-RACB increased barley
537 susceptibility towards *Bgh*, whereas the truncated CA-RACB-ΔCSIL mutant did not. We have
538 shown before in transiently transformed barley cells that removal of the CaaX-box prenylation
539 motif CSIL from RACB results in a shift of CA-RACB's subcellular localization from the plasma
540 membrane to the cytosol and abolishes function in susceptibility (Schultheiss et al., 2003). We
541 have also reported that the interaction of RACB with its downstream effectors mostly takes
542 place at the plant plasma membrane (Schultheiss et al., 2008; Hoefle et al., 2011; McCollum
543 et al., 2020). Our data with CSIL truncations in stable transgenic barley provide now another
544 piece of evidence that ROPs need to be membrane-localized to perform their function, as it
545 has been described before for Arabidopsis (Sorek et al., 2011; Yalovsky, 2015).

546 # Conclusion

547 Regulation of RHO family proteins by PTMs has long been established in the animal research
548 field. In plants, however, we are only at the beginning of discovering these regulatory
549 mechanisms of PTMs in ROP signaling. Here, we present data on *in vivo* ubiquitination of a
550 barley ROP. The identified ubiquitination site is conserved in all ROPs from barley, rice and
551 Arabidopsis, and has been described before for mammalian RACB-homologs. This suggests
552 that the lysine residue corresponding to RACB K167 is a general target for ubiquitination
553 across kingdoms and that this regulates protein abundance.

554 # Experimental procedures

555 ## Heterologous protein expression, purification, and kinase activity
556 measurements

557 A cDNA clone of CA-*RACB* ((Schultheiss et al., 2003), NCBI GenBank identifier for wildtype
558 RACB: CAC83043.2) was cloned into the bacterial expression vector pET26b out of frame of
559 the N-terminal pelB, but in frame with a C-terminal 6xHIS (Novagen, Merck KGaA, Darmstadt,
560 Germany). This way, no potential artificial phosphorylation site was included (Dorjgotov et al.,
561 2009). The barley protein *RBK1* (NCBI GenBank identifier: HE611049.1) was cloned into the
562 pET28a vector in frame with an N-terminal 6xHIS. Cloning was achieved by restriction-ligation
563 after PCR amplification of the cDNA inserts using *Eco*RI and *Xho*I flanking restriction sites on
564 the C- and N-terminal sequence-specific primers. CA-*RACB* was amplified using
565 RACBCA-EcoRI-F + RACBCA-XhoI-R primers, while both wildtype and kinase-dead *RBK1*
566 were amplified with RBK1-F + RBK1-R primers. The kinase dead (KD, K245D) mutant of *RBK1*
567 was constructed by PCR-mediated site-directed mutagenesis using primers RBK1KD-mut-F +
568 RBK1KD-mut-R. After PCR, the parental DNA was digested with *Dpn*I and the whole reaction
569 was transformed into *E. coli* DH5α cells. Following transformation, plasmids were extracted

570 using a routine Miniprep protocol and checked for mutation by sequencing. All primers can be
571 found in S5 Table.

572 Proteins were purified using HisSelect Sepharose beads (Sigma-Aldrich, St. Louis, USA) and
573 the *in vitro* kinase reactions were carried out as described earlier (Huesmann et al., 2012;
574 Reiner et al., 2016). Two parallel reactions, one with and one without radioactive γ-^{32}P-ATP
575 were performed with both WT and KD RBK1, using the same amount of RACB-6xHIS as
576 substrate. The amount of the proteins in the reactions was app. 150 pmol of RACB-6xHIS with
577 4 pmol of 6xHis-RBK1-WT or 12 pmol 6xHis-RBK1-KD. The radioactive reaction for
578 autoradiography contained 10 µM of cold ATP and 0.2 MBq γ-^{32}P-ATP, while 100 µM ATP
579 were included in the non-radioactive reaction destined for mass spectrometry analysis. The
580 reactions were terminated after 2.5 h and proteins were separated on 12% SDS-
581 polyacrylamide gels that were stained by Coomassie Brilliant Blue using standard methods.
582 Radioactive gels were dried and exposed to x-ray films. From the non-radioactive gel, the band
583 containing RACB-6xHIS was cut out and sent for phosphosite mapping.

584 To show stability of both WT and KD 6xHis-RBK1, a routine Ponceau S stain was perfomed.

585 Bioinformatical analysis

586 The putative RACB protein fold was built by homology-modelling using SWISS-MODEL
587 (Waterhouse et al., 2018) with GDP- bound AtROP4 (PDB entry: 2NTY.1 (Thomas et al.,
588 2007)) as template for GDP-bound RACB and GNP-associated *Hs*RAC1 as template for GTP-
589 RACB (PDB entry: 3TH5.1 (Krauthammer et al., 2012)). SWISS-MODEL GMQE (global model
590 quality estimate) scores were 0.75 for GDP-RACB and 0.66 for GTP-RACB, and QMEAN
591 DisCo (qualitative model energy analysis with consensus-based distance constraint) (Studer
592 et al., 2020)) scores were 082 ± 0.07 and 0.80 ± 0.07, respectively. The final RACB models
593 contained amino acids 1-178 for GDP-RACB and 7-178 for GTP-RACB (from 197 total RACB
594 amino acids). PyMOL V2.3.5 (Schrodinger, 2015) was used to generate protein surface
595 structure and cartoon illustrations.

596 All protein sequence alignments were done in Jalview V2.11.0 (Waterhouse et al., 2009) with
597 the MAFFT algorithm running at default settings (Katoh and Toh, 2010). NCBI GenBank
598 identifiers for all aligned proteins are:

599 HvRACB: CAC83043.2; HvRACD: CAD27895.1; HvRAC1: CAD57743.1; HvRAC3:
600 BAJ98596.1; HvROP4: CAD27896.1; HvROP6: CAD27894.1; OsRAC1: XP_015621645.1;
601 OsRAC2: XP_015638759.1; OsRAC3: XP_015625155.1; OsRAC4: XP_015641323.1;
602 OsRAC5: XP_015627011.1; OsRAC6: XP_015625732.1; OsRAC7: XP_015627590.1;
603 AtROP1: NP_190698.1; AtROP2: NP_173437.1; AtROP3: NP_001077910.1; AtROP4:
604 NP_177712.1; AtROP5: NP_195320.1; AtROP6: NP_001190916.1; AtROP9: NP_194624.1;
605 AtROP10: NP_566897.1; AtROP11: NP_201093.1; HsRAC1: NP_001003274.1; HsRHOA:
606 5FR2_A.

607 Generation of transgenic plants

608 A full-length cDNA clone of CA-*RACB* (carrying the G15V mutation as described in
609 (Schultheiss et al., 2003)) and CA-*RACB*-ΔCSIL (lacking the last 4 amino acids, but with an
610 artificial stop codon) were amplified by PCR using primers RACBCA-Esp-Start + RACBCA-
611 Esp-Stop and RACBCA-Esp-Start + RACBCA-ΔCSIL-Esp-Stop, respectively. Both constructs
612 were cloned first into pGGEntL-EP12 and subsequently into pGGInAE-226n_35SP_Ntag-
613 3xHA_35ST vectors using procedures adapted from Golden Gate-based cloning (Engler et al.,
614 2008), generating the 3x*HA*-CA-*RACB*(-ΔCSIL) fusion constructs. From these vectors, the
615 CA-*RACB*(-ΔCSIL) fusion constructs were re-amplified by PCR using primers 3xHA-XmaI-F
616 and RACBCA-XmaI-R (3x*HA*-CA-*RACB*) and 3xHA-XmaI-F + RACBCA-ΔCSIL-XmaI-R
617 (3x*HA*-CA-*RACB*-ΔCSIL). The free 3x*HA*-control was amplified using primers 3xHA-XmaI-F +
618 UL1-XmaI-R. All constructs were introduced into pUbifull-AB-M, a derivative of pNOS-AB-M
619 (DNA-Cloning-Service, Hamburg, Germany) with the maize *POLYUBIQUITIN 1* promoter
620 being inserted in the multiple cloning site, by restriction-ligation using *Xma*I. From there, *Sfi*I
621 fragments were transferred into the generic binary vector p6i-2x35S-TE9 (DNA-Cloning-
622 Service, Hamburg, Germany). The binary plasmids were transferred into *A. tumefaciens* strain

623 AGL1 (Lazo et al., 1991) and transgenic plants were generated by agro-inoculation of
624 immature barley embryos according to Hensel et al. (2009). Transgenic plants were identified
625 by *HYGROMYCIN PHOSPHOTRANSFERASE*-specific PCR, which yielded 47 lines for 3xHA-
626 CA-RACB (BG657 E1-E49; E7 and E41 were not transgenic), 37 lines for 3xHA-CA-RACB-
627 ΔCSIL (BG658 E1-E39; E19 and E38 were not transgenic) and 40 lines for 3xHA (BG659 E1-
628 E42; E17 and E37 were not transgenic). All lines were propagated under normal growth
629 conditions in the greenhouse. Since all descending lines are segregating in generation T_1,
630 individual plants were screened for transgene integration. This was achieved using Western
631 blotting detecting the HA-tag (antibody: Anti-HA-Peroxidase, Sigma-Aldrich, St. Louis, USA,
632 12013819001) and resistance against hygromycin-induced discoloration. For the latter, 7 d old
633 leaves were detached and placed on 0.8% water-agar plates containing 200 µg/ml
634 Hygromycin B (Roth, Karlsruhe, Germany, CP12.2). These plates were put into growth
635 chambers operating under long-day conditions (see below) for roughly 4 d, until discoloration
636 of hygromycin non-resistant plants was observed. After screening, ten positive plants of two
637 lines per construct were picked for an additional round of propagation: we chose BG657 E3
638 and E4 for 3x*HA*-CA-*RACB*, BG658 E4 and E9 for 3x*HA*-CA-*RACB*-ΔCSIL and BG659 E2 and
639 E3 for 3x*HA*. Since the offspring of these lines remained segregating in generation T_2 and no
640 homozygous plants were obtained, all descendants were screened for transgene expression
641 as described above before being used in any experiment. All primers can be found in S5 Table.

642 Plant and fungal growth conditions

643 Transgenic barley (*Hordeum vulgare*) plants of spring-type cultivar Golden Promise were
644 grown under long-day conditions (16 h light, 8 h darkness) with a photon flux of at least 150
645 µmol m^{-2} s^{-1} at 18 °C and a relative humidity of 65%. Transgene-expressing plants of
646 generation T_2 were used in all experiments but one. An exception was made for the *Bgh*
647 penetration assay (see below), because propagation of the T_2 plants was not ready at that
648 time. Therefore, we used corresponding T_1 plants in this experiment. For all other experiments,
649 pools of T_2 plants expressing the same construct were used. For 3x*HA*-CA-*RACB*, we pooled

650 plants of lines BG657 E3 and E4, BG658 E4 and E9 for 3x*HA*-CA-*RACB*-ΔCSIL and BG659
651 E2 and E3 for 3x*HA*. For transient transformation experiments (see below) and propagation of
652 the barley powdery mildew fungus *Blumeria graminis* f.sp. *hordei* race A6 (*Bgh*),
653 non-transformed wildtype barley cultivar Golden Promise plants were grown under the same
654 growth conditions.

655 Assessment of *Bgh* penetration efficiency

656 Primary leaves of transgenic plants were cut and placed on 0.8% water-agar plates. These
657 plates were inoculated with 100-130 spores/mm^2 of *Bgh* and placed under normal growth
658 conditions for 40 h, followed by fixing and destaining leaves in 70% (v/v) ethanol. Fungal
659 spores and appressoria were stained with an ink solution (10% (v/v) Pelikan Ink 4001®
660 (Pelikan, Hannover, Germany), 25% (v/v) acetic acid) and analyzed by transmission light
661 microscopy. Haustorium establishment was counted as successful penetration, while stopped
662 fungal growth after appressorium formation was counted as successful plant defense. For each
663 construct, three transgene-expressing plants of one T_1 line (BG657 E4 for 3x*HA*-CA-*RACB*,
664 BG658 E4 for 3x*HA*-CA-*RACB*-ΔCSIL and BG659 E2 for 3x*HA*) were analyzed, with at least
665 96 evaluated plant-fungus interaction sites per plant.

666 For the analysis of *Bgh* susceptibility after transient overexpression of untagged CA-RACB(-
667 K167R), a full-length cDNA clone of *RACB* was first amplified with Gateway® attachment sites
668 using primers RACB-Gateway-F + RACB-Gateway-R and cloned into the Gateway® entry
669 vector pDONR223 using routine Gateway® BP-cloning procedures (Invitrogen, Carlsbad,
670 California, USA). From pDONR223, *RACB* was transferred into the Gateway®-compatible
671 plant expression vector pGY1-GW (generated in Engelhardt et al. (2019)) using routine
672 Gateway® LR-cloning. A CA-*RACB*-K167R clone was generated from pGY1-*RACB* using
673 subsequent site-directed mutagenesis with primers RACB-SDM-G15V-F + RACB-SDM-G15V-
674 R and RACB-SDM-K167R-F + RACB-SDM-K167R-R. Integrity of the sequences and
675 mutations was confirmed via Sanger sequencing. All primers can be found in S5 table.

676 For transient transformation via particle bombardment, three primary leaves of 7 d old wildtype
677 barley plants (cultivar Golden Promise) were placed on 0.8% water-agar plates and
678 transformed using the PDS-1000/He™ system (Bio-Rad, Hercules, California, USA). For one
679 transformation reaction, 11 µl of 25 mg/ml spherical gold particles (diameter 1 µm, Nanopartz,
680 Loveland, USA) were mixed with 1 µg plasmid DNA coding for pGY1-CA-*RACB*, pGY1-CA-
681 *RACB*-K167R or pGY1 (empty) and 0.5 µg plasmid DNA coding for the transformation marker
682 pUbi-*GUSplus* (a gift from Claudia Vickers, Addgene plasmid #64402,
683 http://n2t.net/addgene:64402, (Vickers et al., 2003)). Afterwards, 15 µl $CaCl_2$ (to a final
684 concentration of 0.5 M) and 7.5 µl of 20 mg/ml Protamine (Sigma-Aldrich, St. Louis, USA) were
685 added and the solution was incubated at RT for 30 min, with occasional mixing. Subsequently,
686 the solution was washed twice, first with 500 µl 70% ethanol and second with 500 µl 100%
687 ethanol. Finally, the gold particles were dissolved in 6 µl 100% ethanol using a sonicator and
688 used in the PDS-1000/He™ System. For each plasmid combination, nine barley leaves
689 distributed on three plates were transiently transformed per biological replicate. After
690 transformation, all plates were placed in a growth chamber operating under the above stated
691 conditions. These plates were then challenge-inoculated with 100-130 spores/mm^2 of *Bgh* at
692 24 h post transformation and incubated under normal plant growth condition for 40 h.
693 Afterwards, the leaves were first transferred into plates containing a GUS-staining solution
694 (0.1 M Na_2HPO_4/NaH_2PO_4 buffer pH 7, 0.01 M sodium EDTA, 0.005 M potassium
695 hexacyanoferrat (II), 0.005 M potassium hexacyanoferrat (III), 0.1% (v/v) Triton X-100, 20%
696 (v/v) methanol, 0.5 mg/ml X-gluc (1,5-bromo-4-chloro-3-indoxyl-β-D-glucuronic acid,
697 cyclohexylammonium salt (Carbosynth, Bratislava, Slovak Republic), (Schweizer et al., 1999)),
698 vacuum infiltrated for 3 min and incubated at 37 °C for 6 h in the dark, before finally being
699 destained in 70% ethanol. For analysis of fungal penetration efficiency, fungal material was
700 stained using a calcofluor staining solution (0.3% (w/v) Calcufluor-white, 50 mM Tris pH 9)
701 before being subjected to light microscopy. Briefly, leaves were screened for transformed cells,
702 which could be distinguished due to their blue GUS-stain. If a fungal attack occurred in a
703 transformed cell, established haustoria were counted as successful penetration, while halted

704 fungal growth after appressorium formation was counted as successful plant defense. The *Bgh*
705 penetration efficiency for each plasmid combination was calculated by dividing the number of
706 successful penetration events by the sum of all successful penetration and defense events in
707 this combination. Five biological replicates of this experiment were analyzed, with at least 50
708 evaluated plant-fungus interactions per plasmid combination per replicate. Fig 8 displays all
709 *Bgh* penetration efficiencies divided by the mean penetration efficiency of all empty vector
710 controls with the respective standard error of the mean. All penetration efficiency data (stable
711 and transient assays) were visualized with GraphPad Prism version 6. Statistical analysis was
712 performed in RStudio V1.2.5033 (source: https://rstudio.com/) using R V3.6.3 (source:
713 https://www.R-project.org). Normal distribution and homogeneity of variance in the datasets
714 were confirmed with Shapiro-Wilk's test and Levene's test, respectively. Significant differences
715 of results were assessed using a One-way ANOVA with Tukey's HSD against a p-value of
716 0.05.

717 Protoplast transformation, proteasome inhibition and protein 718 extraction

719 Transgenic barley protoplasts stably expressing 3xHA-CA-RACB (pools of lines BG657 E3
720 and E4) or 3xHA (pools of lines BG659 E2 and E3) were isolated and super-transformed as
721 described in Reiner et al. (2016), with the following deviations: transformation reactions were
722 scaled to 1 ml of protoplasts and overnight incubation was conducted in 1 ml buffer WI in single
723 cell culture tubes. For transformation, 50 µg/ reaction of a plasmid coding for *GFP-RBK1* (from
724 Huesmann et al. (2012)) or water (as a mock control) were used. Ten reactions per
725 combination (S2A and S2B Figs) were prepared. After overnight incubation, MG132 was
726 added to a final concentration of 10 µM, followed by incubation in the dark for 3 h. Protoplasts
727 of corresponding reactions were pooled and pelleted by centrifugation at 120 g. Supernatants
728 were removed and protoplasts were lysed by brief vortexing and snap-freezing in liquid
729 nitrogen. Proteins were resuspended in a modified extraction buffer (10% (w/v) glycerol, 25
730 mM Tris pH 7.5, 150 mM NaCl, 10 mM DTT, 1 mM PMSF, 1% sodium deoxycholate, 1x

731 protease inhibitor (Sigma-Aldrich, St. Louis, USA, P9599), 1 tablet /10 ml PhosSTOP™
732 (Sigma-Aldrich, St. Louis, USA, 4906845001)) and incubated on ice for 30 min with occasional
733 mixing. This solution was centrifuged at 4 °C to pellet cell debris, the supernatant was digested
734 with trypsin and used in phosphopeptide enrichment (S2A Fig (center panel) and S3B Fig). In
735 one experiment, where the phosphopeptide enrichment was skipped (S2A Fig (bottom panel)),
736 proteins were subjected to immunoprecipitation (see below), loaded on a SDS-PAGE and then
737 submitted to in-gel tryptic digest prior to mass spectrometry. All buffers described in the
738 immunoprecipitation paragraph were used. In another experiment (S2A Fig (top panel)),
739 protoplast lysates were subjected to immunoprecipitation using a modified extraction buffer
740 (10% (w/v) glycerol, 25 mM Tris pH 7.5, 150 mM NaCl, 10 mM DTT, 1 mM PMSF, 50 µM
741 MG132, 1x protease inhibitor (Sigma-Aldrich, St. Louis, USA, P9599), 1 tablet /10 ml
742 PhosSTOP™ (Sigma-Aldrich, St. Louis, USA, 4906845001)) and washing buffer (10% (w/v)
743 glycerol, 25 mM Tris pH 7.5, 150 mM NaCl, 1 mM PMSF, 50 µM MG132, 1x protease inhibitor
744 (Sigma-Aldrich, St. Louis, USA, P9599), 1 tablet /10 ml PhosSTOP™ (Sigma-Aldrich, St.
745 Louis, USA, 4906845001)) and used for on-bead tryptic digest prior to phosphopeptide
746 enrichment via IMAC.

747 Immunoprecipitation and Western blotting

748 In order to show protein stability of 3x*HA*-CA-*RACB* and 3x*HA*-CA-*RACB*-ΔCSIL, we
749 performed a routine αHA-immunoprecipitation from untreated transgenic leaves (lines BG657
750 E3 and E4 and BG658 E4 and E9, respectively), followed by an anti-HA Western blot (see
751 below). For ubiquitination analysis, transgenic barley leaves expressing 3xHA-CA-RACB (lines
752 BG657 E3 and E4) or 3xHA (lines BG659 E2 and E3) were vacuum infiltrated for 3 min at -26
753 mm in Hg with a leaf-floating solution (0.45 M mannitol, 10 mM MES pH 5.7, 10 mM $CaCl_2$,
754 0.0316 g /10 ml Gamborg B5 medium including vitamins (Duchefa, RV Haarlem, The
755 Netherlands, G0210), 50 µM MG132). To determine, whether the observed ubiquitin-like
756 laddering pattern of 3xHA-CA-RACB is MG132-dependent, we floated transgenic barley
757 leaves expressing 3xHA-CA-RACB (lines BG657 E3 and E4) either on the float solution

758 described above or in a solution that contained the equal volume of DMSO instead of MG132.
759 After incubation in the dark for 3 h, leaves were snap-frozen in liquid nitrogen and homogenized
760 using a TissueLyser II (QIAGEN, Hilden, Germany). Proteins were resuspended in extraction
761 buffer (10% (w/v) glycerol, 25 mM Tris pH 7.5, 1 mM EDTA, 150 mM NaCl, 10 mM DTT, 1 mM
762 PMSF, 0.5% Nonidet P40 substitute, 1x protease inhibitor (Sigma-Aldrich, St. Louis, USA,
763 P9599)) by tumbling end-over-end at 4 °C for 30 min. Cell debris was removed by
764 centrifugation and the supernatants were used for immunoprecipitation (IP). IPs were
765 conducted according to routine procedures. Briefly, for each sample, 50 µM Pierce™ Anti-HA
766 Magnetic Beads (Thermo Fisher Scientific, Waltham, USA) were equilibrated 3x in extraction
767 buffer before adding supernatants. HA-tagged proteins were immunoprecipitated by tumbling
768 end-over-end for 1 h at 4 °C, then washed 5x with washing buffer (10% (w/v) glycerol, 25 mM
769 Tris pH 7.5, 1 mM EDTA, 150 mM NaCl, 1 mM PMSF, 1x protease inhibitor (Sigma-Aldrich,
770 St. Louis, USA, P9599)). For selected RACB phosphopeptide screenings (S2A Fig), the beads
771 were directly prepared for mass spectrometry. Otherwise, proteins were eluted in 100 µl of 2x
772 NuPAGE™ LDS Sample Buffer (Thermo Fisher Scientific, Waltham, USA, NP0008) and boiled
773 at 95 °C for 10 min. After the IP, 25 µl of eluate were separated on a 12% SDS-PAGE and
774 proteins were transferred to a PVDF membrane. HA-tagged proteins were detected with an
775 Anti-HA-Peroxidase antibody (Sigma-Aldrich, St. Louis, USA, 12013819001). For the RACB
776 ubiquitination screening, the remaining 75 µl were loaded on another 12% SDS-PAGE and
777 silver stained after separation. For this, the SDS-PAGE was incubated in a fixation solution
778 (50% (v/v) methanol, 5% (v/v) acetic acid, 45% (v/v) water) for 1 h and subsequently washed
779 with water three times (two times 2 min each, last time 1 h) on a shaking incubator. The gel
780 was sensitized with a 0.02% (w/v) sodium thiosulfate solution for 2 min, then briefly washed
781 with water twice. Afterwards, the gel was incubated at 4 °C in pre-chilled 0.1% (w/v) silver
782 nitrate for 30 min, then rinsed two times with water for 30 s each. In order to stain proteins, the
783 gel was incubated in a developing solution (0.04% (v/v) formaldehyde in 2% (w/v) sodium
784 carbonate) until a sufficient degree of staining had been obtained. Then, the gel was washed
785 five times in 1% (v/v) acetic acid to stop the reaction. Bands corresponding to 3xHA-CA-RACB

786 and its higher molecular weight derivatives were excised from the gel and the gel slices were
787 prepared for mass spectrometry. In order to show protein stability of 3x*HA*-CA-*RACB* and
788 3x*HA*-CA-*RACB*-ΔCSIL, we performed a routine HA-immunoprecipitation from untreated
789 transgenic leaves (lines BG657 E3 and E4 and BG658 E4 and E9, respectively), followed by
790 an αHA Western blot.

791 Protein digest and phosphopeptide enrichment

792 In-gel digestion of SDS-PAGE gel segments was performed according to standard
793 procedures. Briefly, excised gel segments were reduced and alkylated with 10 mM
794 dithiothreitol (DTT) and 55 mM chloroacetamide (CAA) followed by digestion with
795 trypsin (Roche). Dried peptides were reconstituted with 0.1% FA in water prior to LC-MS
796 analysis. For peptide retention time monitoring, PROCAL peptide standard (Zolg et al.,
797 2017) was added to peptide mixtures at a concentration of 100 fmol on column.

798 On-bead digestion of one immunoprecipitation sample (from the experiment described in S2A
799 Fig (bottom panel)) was performed to facilitate a subsequent phosphopeptide enrichment. Dry
800 beads-bound proteins were incubated with urea buffer (8 M Urea, 50 mM Tris HCl pH 8.5, 10
801 mM DTT, cOmplete™ EDTA-free protease inhibitor cocktail (PIC) (Roche, Basel, Switzerland,
802 04693132001), Phosphatase inhibitor (PI-III; in-house, composition resembling Phosphatase
803 inhibitor cocktail 1 (P2850), 2 (P5726) and 3 (P0044) from Sigma-Aldrich, St. Louis, USA) for
804 one hour at 30 °C. The sample was alkylated (55 mM CAA), diluted 1:8 with digestion buffer
805 (50 mM Tris-HCl pH 8.5, 1 mM $CaCl_2$) and pre-digested with trypsin (1:100 protease:protein
806 ratio) for 4 hours followed by overnight digestion with trypsin (1:100 protease:protein ratio) at
807 37 °C. The sample was acidified to pH 3 with TFA and centrifuged at 14,000 *g* for 15 min at
808 4°C. The supernatant was desalted on a 50 mg SepPAC column (Waters, Milford, USA; elution
809 buffer 50% acetonitrile, 0.07% TFA).

810 Proteins from protoplast lysates were precipitated overnight with 10% trichloroacetic acid in
811 ice-cold acetone at -20°C. Precipitates were washed two times with ice-cold acetone and dry

812 samples re-suspended in urea buffer (8 M Urea, 50 mM Tris HCl pH 8.5, 1 mM DTT,
813 cOmpleteTM EDTA-free protease inhibitor cocktail (PIC) (Roche, Basel, Switzerland,
814 04693132001), Phosphatase inhibitor (PI-III; in-house, composition resembling Phosphatase
815 inhibitor cocktail 1 (P2850), 2 (P5726) and 3 (P0044) from Sigma-Aldrich, St. Louis, USA).

816 Protein concentration was determined with the Bradford assay (Bradford, 1976). 200 µg
817 (experiment described in S2A Fig (center panel)) or 900 µg (all experiments described in S2B
818 Fig) total protein was reduced (10 mM DTT), alkylated (55 mM CAA), diluted 1:8 with digestion
819 buffer and pre-digested with trypsin (1:100 protease:protein ratio) for 4 hours followed by
820 overnight digestion with trypsin (1:100 protease:protein ratio) at 37 °C. Samples were acidified
821 to pH 3 with TFA and centrifuged at 14,000 *g* for 15 min at 4 °C. Supernatants were desalted
822 on 50 mg SepPAC columns (Waters; elution buffer 50% acetonitrile, 0.07% TFA).

823 Phosphopeptide enrichment was performed using a Fe^{3+}-IMAC column (Propac IMAC-10 4x50
824 mm, Thermo Fisher Scientific, Waltham, USA) as described previously (Ruprecht et al.,
825 2017b). Shortly, desalted peptide samples were adjusted to 30% acetonitrile, 0.07% TFA. For
826 quality control, 1.5 nmol of a synthetic library of phosphopeptides and their corresponding non-
827 phosphorylated counterpart sequence (F1) (Marx et al., 2013), were spiked into samples prior
828 to loading onto the column. The enrichment was performed with buffer A (0.07% TFA,
829 30% acetonitrile) as wash buffer and Buffer B (0.315% NH_4OH) as elution buffer. Collected full
830 proteome and phosphopeptide fractions were vacuum-dried and stored at -80°C until further
831 use.

832 Phosphopeptides from the experiments described in S2A Fig (top and center panels) were re-
833 suspended in 50 mM citrate, 0.1% formic acid (FA) and desalted on self-packed StageTips
834 (five disks, Ø 1.5 mm C18 material, 3M Empore™, elution solvent 0.1% FA in 50% ACN).
835 Phosphopeptides from the experiment described in S2B Fig were re-suspended in 50 mM
836 citrate, 0.1% formic acid (FA), fractionated on basic reverse phase StageTip microcolumns
837 (five disks, Ø 1.5 mm C18 material, 3M Empore™) and pooled to 4 fractions, as described

838 previously (Ruprecht et al., 2017a). Dried peptides were reconstituted with 0.1% FA in water
839 prior to LC-MS analysis.

840 *In vitro* kinase assay samples were mixed 1:4 with urea buffer (8 M urea, 50 mM Tris-
841 HCl pH 7.5). Samples were reduced (5 mM DTT, 1h, room temperature), alkylated (15 mM
842 CAA, 30 min, room temperature) and subsequently diluted 1:8 with digestion buffer. In-solution
843 pre-digestion with trypsin (Roche, Basel, Switzerland) was performed for 4 hours at 37 °C (1:50
844 protease:protein ratio), followed by overnight digestion with trypsin (1:50 protease:protein
845 ratio). Samples were acidified to pH 3 using trifluoroacetic acid (TFA) and centrifuged at
846 14,000 *g* for 5 min. The supernatant was desalted on self-packed StageTips (four disks, Ø 1.5
847 mm C18 material, 3M Empore™, elution solvent 0.1% FA in 50% ACN). Dried peptides were
848 reconstituted with 0.1% FA in water prior to LC-MS analysis.

849 Mass spectrometry

850 Liquid chromatography-coupled mass spectrometry (LC-MS/MS) analysis was
851 performed on Orbitrap mass spectrometer systems (Thermo Fisher Scientific, Waltham,
852 USA) coupled on-line to a Dionex 3000 HPLC (Thermo Fisher Scientific, Waltham, USA).
853 The liquid chromatography setup consisted of a 75 µm × 2 cm trap column packed in-
854 house with Reprosil Pur ODS-3 5 µm particles (Dr. Maisch GmbH) and a 75 µm × 40 cm
855 analytical column, packed with 3 µm particles of C18 Reprosil Gold 120 (Dr. Maisch GmbH,
856 Ammerbuch, Germany). Peptides were loaded onto the trap column using 0.1% FA in water.
857 Separation of the peptides was performed by using a linear gradient from 4% to 32% ACN with
858 5% DMSO, 0.1% formic acid in water over 60 min followed by a washing step (70 min total
859 method length) at a flow rate of 300 nl/min and a column temperature of 50 °C. For
860 phosphopeptide fractions, the gradient was adjusted to a two-step gradient from 4% to
861 27% ACN. The instruments were operated in data-dependent mode, automatically switching
862 between MS and MS2 scans.

863 For the RACB ubiquitination screen samples (S2C Fig), full-scan mass spectra (m/z
864 360-1300) were acquired in profile mode on a Q Exactive HF with 60,000 resolution, an
865 automatic gain control (AGC) target value of 3e6 and 10 ms maximum injection time. For the
866 top 20 precursor ions, high resolution MS2 scans were performed using HCD fragmentation
867 with 25% normalized collision energy, 30,000 resolution, an AGC target value of 2e5, 50 ms
868 maximum injection time and 1.7 *m/z* isolation width in centroid mode. The underfill ratio was
869 set to 1% with a dynamic exclusion of 20 s. To confirm and more precisely monitor the GlyGly-
870 and phospho-modified peptides identified in the global analysis of these samples, a targeted
871 parallel reaction monitoring assay (PRM) was set up on the Q Exactive HF using the same LC
872 gradient settings. Peptide precursor charge states were chosen based on the previous
873 identification results. In addition, a selection of PROCAL retention time calibration mixture
874 peptides was monitored. PRM measurements were performed with the acquisition method
875 switching between experiments after one duty-cycle. The first experiment consisted of a full
876 scan MS1 spectrum recorded in the Orbitrap (360 to 1300 m/z, 15k resolution, AGC target
877 3e6, Maximum IT 50 ms). The second experiment consisted of a tMS2 PRM scan triggering
878 MS2 scans based on a list containing retention time window, m/z and charge information. For
879 the tMS2 PRM scan, the scheduled precursors were isolated (isolation window 1.3 m/z),
880 fragmented via HCD (NCE 25%) and recorded in the Orbitrap (120 to 2,000 m/z, 15k
881 resolution, AGC target 2e5, Maximum IT 100 ms).
882 For the kinase assay samples, full scan maximum injection time was 50 ms and MS2 scans
883 were performed with a resolution of 15,000 and 100 ms maximum injection time. His-tagged
884 CA-RACB and RBK1 peptides were set on an inclusion list and the dynamic exclusion set to
885 5s.
886 For the experiments described in S2B Fig, full-scan mass spectra (m/z 360-1300) were
887 acquired in profile mode on a Q Exactive HF-X with 60,000 resolution, an automatic gain
888 control (AGC) target value of 3e6 and 45 ms maximum injection time. For the top 20 precursor
889 ions, high resolution MS2 scans were performed using HCD fragmentation with 26 %
890 normalized collision energy, 30,000 resolution, an AGC target value of 2e5, and 1.3 *m/z*

891 isolation width in centroid mode. The intensity threshold was set to 2.2e4 with a dynamic
892 exclusion of 25 s. RACB and RBK1 peptides were set on an inclusion list. Full proteome
893 samples were measured with 50 ms maximum injection time for MS2 scans, phosphopeptide
894 samples with 100 ms.
895 For the experiment described in S2A Fig, full-scan mass spectra (m/z 360-1,300) were
896 acquired in profile mode on an Orbitrap Fusion LUMOS with 60,000 resolution, an
897 automatic gain control (AGC) target value of 4e5 and 50 ms maximum injection time. For the
898 top 15 precursor ions, high resolution MS2 scans were performed using HCD fragmentation
899 with 30% normalized collision energy, 30,000 resolution, an AGC target value of 5e4, 120 ms
900 maximum injection time and 1.7 *m/z* isolation width in centroid mode. The intensity threshold
901 was set to 2.5e4 with a dynamic exclusion of either 27 s (all peptides) or 10 s (RACB peptides
902 set on an inclusion list).
903 Peptide and protein identification and quantification was performed with MaxQuant (Cox and
904 Mann, 2008) using standard settings (version 1.5.8.3). Raw files were searched against a
905 barley database (160517_Hv_IBSC_PGSB_r1_proteins_HighConf_REPR_annotation.fasta;
906 IPK Gatersleben) and common contaminants. For the experiments described in S2B Fig,
907 we added the phosphopeptide library sequences (Marx et al., 2013). For the kinase assay
908 dataset, we used the recombinant protein sequences and an *E. coli* reference database
909 (uniprot-proteome_UP000000625). Carbamidomethylated cysteine was set as fixed
910 modification and oxidation of methionine, and N-terminal protein acetylation as variable
911 modifications. Lysine ubiquitylation, phosphorylation of serine, threonine or tyrosine were set
912 as variable modification were applicable. An m/z value of 115.0502 was specified as diagnostic
913 ion for lysine glyglycylation (Zolg et al., 2018). Trypsin/P was specified as the proteolytic
914 enzyme, with up to two missed cleavage sites allowed. The match between run function was
915 enabled for matching samples and between fractions. Results were filtered to 1% PSM, protein
916 and Site FDR. MS spectra were displayed with MaxQuant viewer.
917 RAW files from the PRM measurement of the ubiquitination screen samples were imported
918 into Skyline (64-bit, v.4.1.0.11796) (MacLean et al., 2010) for data filtering and analysis and

919 transition selection was manually refined to include site determining ions for each modification
920 site. Peaks were integrated using the automatic peak finding function followed by manual
921 curation of all peak boundaries and transitions. The summed area under the fragment ion
922 traces data for every transition was exported for data visualization in Microsoft Excel and used
923 to confirm the expected relative quantity of modified RACB peptides based on the gel segment.
924 The mass spectrometry proteomics data have been deposited to the ProteomeXchange
925 Consortium via the PRIDE (Vizcaíno et al., 2016) partner repository with the dataset identifier
926 PXD019273.

927 Confocal microscopy

928 For the generation of GFP-tagged RACB-variants, *RACB* coding sequence was mutated in
929 pDONR223-*RACB* (from above) to create the G15V (CA), T20N (DN), K167R, G15V-K167R
930 and T20N-K167R mutants using site-directed mutagenesis with the respective primer pairs
931 RACB-SDM-G15V-F + RACB-SDM-G15V-R, RACB-SDM-T20N-F + RACB-SDM-T20N-R and
932 RACB-SDM-K167R-F + RACB-SDM-K167R-R. Subsequently, the *RACB* mutants were
933 transferred from pDONR223 into the Gateway®-compatible plant expression vector pGY1-
934 *GFP* (described in Engelhardt et al. (2019)) via Gateway® LR-cloning. Integrity of the
935 sequences and mutations were confirmed via Sanger sequencing. All primers can be found in
936 S5 Table. Protein stability of GFP-tagged RACB and its variants (WT, CA, DN and WT-K167R,
937 CA-K167R, DN-K167R) was indirectly assessed in transiently transformed barley epidermal
938 cells using confocal laser-scanning microscopy. For this, three primary leaves of 7 d old
939 wildtype barley plants (cultivar Golden Promise) were placed on 0.8% water-agar plates and
940 transformed using biolistic bombardment with the PDS-1000/He™ system (Bio-Rad, Hercules,
941 California, USA) as described above. For one transformation reaction, 1 µg of plasmid DNA
942 coding for a GFP-tagged RACB variant and 0.5 µg of plasmid DNA coding for free mCherry
943 were mixed. At 24 h post transformation, the leaves were analyzed using a Leica TCS SP5
944 CLSM mounted on a DM6000 stage (Leica, Wetzlar, Germany). Single transformed barley
945 epidermal cells were identified and fluorophores were sequentially scanned. Hereby, GFP was
946 excited with a 488 nm Argon laser and detected between 500 nm and 550 nm using a HyD

947 detector, while mCherry was excited with a 561 nm laser line and detected between 570 nm
948 and 620 nm using another HyD detector. To analyze and compare fluorescence intensities
949 between one RACB variant and its K167R counterpart, appropriate laser and detector settings
950 were chosen initially and kept constant for all cells and biological replicates of this combination.
951 For all cells, Z-stacks with 2 µm step size were acquired, ranging from the top of the cell until
952 the full nucleus was captured. The number of Z-stacks was kept constant for each RACB
953 variant combination. For one biological replicate, at least 25 cells were imaged per construct,
954 with three biological replicates in total. Single-cell mean pixel fluorescence intensities were
955 measured separately for GFP and mCherry, as 8 bit grey scale values using Fiji (Schindelin et
956 al., 2012), with regions of interest (ROIs) over one whole cell that was displayed a maximum
957 intensity projection of the Z-stacks. Data points of three independent experiments were
958 collected and graphed in GraphPad Prism version 6. Statistical analysis was performed in
959 RStudio V1.2.5033 (source: https://rstudio.com/) using R V3.6.3 (source: https://www.R-
960 project.org). Normal distribution and homogeneity of variance were tested with Shapiro-Wilk's
961 test and *Fisher's*-test, respectively. Significant differences of results were assessed using
962 Wilcoxon's rank-sum test with continuity correction against a p-value of 0.05.

963 For the RIC171 recruitment assay, an mCherry-RIC171 clone was generated by first amplifying
964 a coding sequence of *RIC171* (Schultheiss et al., 2008) via PCR with the primer pair RIC171-
965 Gateway-F + RIC171-Gateway-R and cloning it into the Gateway® entry vector pDONR223
966 using Gateway® BP-cloning. From there, RIC171 was transferred into the Gateway®-
967 compatible plant expression vector pGY1-nmCherry (generated in Engelhardt et al. (2019))
968 using Gateway® LR-cloning to create pGY1-*mCherry-RIC171*. For transient transformation of
969 barley epidermal cells, 1 µg of pGY1-*mCherry-RIC171* was mixed with 1 µg of pGY1-*CFP* and
970 either 0.5 µg of pGY1-*GFP*, 1 µg of pGY1-*GFP*-CA-*RACB* or 1 µg of pGY1-*GFP*-CA-*RACB*-
971 K167R for one reaction. Transient transformation of 7 d old wildtype barley plants (cultivar
972 Golden Promise) was carried out as described above. Single epidermal cells were analyzed
973 24 h after transformation using the Leica TCS SP5. CFP was excited with the 458 nm Argon
974 laser line and detected between 463 nm and 485 nm using a HyD detector, while GFP was

975 excited with the 488 nm Argon laser line and detected between 500 nm and 550 nm using a
976 PMT and mCherry was excited with the 561 nm laser line and detected between 570 nm and
977 620 nm using another HyD detector. Individual laser excitation strengths and detector
978 sensitivity settings were used for each cell in order to give high quality images. For all cells,
979 sequentially-scanned Z-stacks with 2 µm step size were taken, ranging from the top of the cell
980 until the full nucleus was captured, with the number of Z-steps being unique for each cell. For
981 each combination of constructs, 15 cells were taken per replicate, with 3 biological replicates
982 in total. For better illustration, the brightness of the representative images in this study was
983 enhanced post scanning using the Leica Application Suite X software V3.5.7.23225 (Leica,
984 Wetzlar, Germany).

985 # Acknowledgements

986 We acknowledge the technical assistance of Cornelia Marthe (IPK Gatersleben) in generating
987 the transgenic barley used in this study and Dalma Ménesi for her help with protein purifications
988 (IPB, BRC Szeged). We are grateful to the TUM plant technology center for support in
989 propagation of transgenic barley plants.

990

991 # References

992 **Abdrabou, A., and Wang, Z.** (2018). Post-translational modification and subcellular distribution of
993 Rac1: An update. Cells **7,** 263.
994 **Abdul-Manan, N., Aghazadeh, B., Liu, G.A., Majumdar, A., Ouerfelli, O., Siminovitch, K.A., and Rosen,**
995 **M.K.** (1999). Structure of Cdc42 in complex with the GTPase-binding domain of the 'Wiskott–
996 Aldrich syndrome'protein. Nature **399,** 379-383.
997 **Akamatsu, A., Wong, H.L., Fujiwara, M., Okuda, J., Nishide, K., Uno, K., Imai, K., Umemura, K.,**
998 **Kawasaki, T., and Kawano, Y.** (2013). An OsCEBiP/OsCERK1-OsRacGEF1-OsRac1 module is an
999 essential early component of chitin-induced rice immunity. Cell host & microbe **13,** 465-476.
1000 **Berken, A.** (2006). ROPs in the spotlight of plant signal transduction. Cell Mol Life Sci **63,** 2446-2459.
1001 **Berken, A., and Wittinghofer, A.** (2008). Structure and function of Rho-type molecular switches in
1002 plants. Plant Physiol Biochem **46,** 380-393.
1003 **Berken, A., Thomas, C., and Wittinghofer, A.** (2005). A new family of RhoGEFs activates the Rop
1004 molecular switch in plants. Nature **436,** 1176-1180.
1005 **Boulter, E., and Garcia-Mata, R.** (2010). RhoGDI: A rheostat for the Rho switch. Small GTPases **1,** 65-
1006 68.
1007 **Bradford, M.M.** (1976). A rapid and sensitive method for the quantitation of microgram quantities of
1008 protein utilizing the principle of protein-dye binding. Anal Biochem **72,** 248-254.
1009 **Castillo-Lluva, S., Tan, C.T., Daugaard, M., Sorensen, P.H., and Malliri, A.** (2013). The tumour
1010 suppressor HACE1 controls cell migration by regulating Rac1 degradation. Oncogene **32,** 1735-
1011 1742.
1012 **Chang, F., Lemmon, C., Lietha, D., Eck, M., and Romer, L.** (2011). Tyrosine phosphorylation of Rac1: a
1013 role in regulation of cell spreading. PLoS One **6,** e28587.
1014 **Cox, J., and Mann, M.** (2008). MaxQuant enables high peptide identification rates, individualized ppb-
1015 range mass accuracies and proteome-wide protein quantification. Nature biotechnology **26,**
1016 1367-1372.
1017 **Dong, S., Zhao, J., Wei, J., Bowser, R.K., Khoo, A., Liu, Z., Luketich, J.D., Pennathur, A., Ma, H., and**
1018 **Zhao, Y.** (2014). F-box protein complex FBXL19 regulates TGFbeta1-induced E-cadherin down-
1019 regulation by mediating Rac3 ubiquitination and degradation. Mol Cancer **13,** 76.
1020 **Dorjgotov, D., Jurca, M.E., Fodor-Dunai, C., Szűcs, A., Ötvös, K., Klement, É., Bíró, J., and Fehér, A.**
1021 (2009). Plant Rho-type (Rop) GTPase-dependent activation of receptor-like cytoplasmic
1022 kinases in vitro. FEBS Letters **583,** 1175-1182.
1023 **Ebine, K., Fujimoto, M., Okatani, Y., Nishiyama, T., Goh, T., Ito, E., Dainobu, T., Nishitani, A., Uemura,**
1024 **T., Sato, M.H., Thordal-Christensen, H., Tsutsumi, N., Nakano, A., and Ueda, T.** (2011). A
1025 membrane trafficking pathway regulated by the plant-specific RAB GTPase ARA6. Nat Cell Biol
1026 **13,** 853-859.
1027 **Ellerbroek, S.M., Wennerberg, K., and Burridge, K.** (2003). Serine phosphorylation negatively
1028 regulates RhoA in vivo. J Biol Chem **278,** 19023-19031.
1029 **Enders, T.A., Frick, E.M., and Strader, L.C.** (2017). An Arabidopsis kinase cascade influences auxin-
1030 responsive cell expansion. Plant J **92,** 68-81.
1031 **Engelhardt, S., Kopischke, M., Hofer, J., Probst, K., McCollum, C., and Hückelhoven, R.** (2019). Barley
1032 RIC157 is involved in RACB-mediated susceptibility to powdery mildew. bioRxiv**,** 848226.
1033 **Engler, C., Kandzia, R., and Marillonnet, S.** (2008). A one pot, one step, precision cloning method with
1034 high throughput capability. PLoS One **3,** e3647.
1035 **Fodor-Dunai, C., Fricke, I., Potocky, M., Dorjgotov, D., Domoki, M., Jurca, M.E., Otvos, K., Zarsky, V.,**
1036 **Berken, A., and Feher, A.** (2011). The phosphomimetic mutation of an evolutionarily
1037 conserved serine residue affects the signaling properties of Rho of plants (ROPs). Plant J **66,**
1038 669-679.

1039 **Forget, M.-A., Desrosiers, R.R., Gingras, D., and Béliveau, R.** (2002). Phosphorylation states of Cdc42
1040 and RhoA regulate their interactions with Rho GDP dissociation inhibitor and their extraction
1041 from biological membranes. Biochemical Journal **361,** 243-254.
1042 **Fricke, I., and Berken, A.** (2009). Molecular basis for the substrate specificity of plant guanine
1043 nucleotide exchange factors for ROP. FEBS letters **583,** 75-80.
1044 **Gohre, V., Spallek, T., Haweker, H., Mersmann, S., Mentzel, T., Boller, T., de Torres, M., Mansfield,**
1045 **J.W., and Robatzek, S.** (2008). Plant pattern-recognition receptor FLS2 is directed for
1046 degradation by the bacterial ubiquitin ligase AvrPtoB. Curr Biol **18,** 1824-1832.
1047 **Hensel, G., Kastner, C., Oleszczuk, S., Riechen, J., and Kumlehn, J.** (2009). Agrobacterium-mediated
1048 gene transfer to cereal crop plants: current protocols for barley, wheat, triticale, and maize.
1049 Int J Plant Genomics **2009,** 835608.
1050 **Hoefle, C., Huesmann, C., Schultheiss, H., Börnke, F., Hensel, G., Kumlehn, J., and Hückelhoven, R.**
1051 (2011). A barley ROP GTPase ACTIVATING PROTEIN associates with microtubules and regulates
1052 entry of the barley powdery mildew fungus into leaf epidermal cells. The Plant Cell **23,** 2422-
1053 2439.
1054 **Hua, Z., and Vierstra, R.D.** (2011). The cullin-RING ubiquitin-protein ligases. Annu Rev Plant Biol **62,**
1055 299-334.
1056 **Huesmann, C., Reiner, T., Hoefle, C., Preuss, J., Jurca, M.E., Domoki, M., Feher, A., and Huckelhoven,**
1057 **R.** (2012). Barley ROP binding kinase1 is involved in microtubule organization and in basal
1058 penetration resistance to the barley powdery mildew fungus. Plant Physiol **159,** 311-320.
1059 **Irani, K., Xia, Y., Zweier, J.L., Sollott, S.J., Der, C.J., Fearon, E.R., Sundaresan, M., Finkel, T., and**
1060 **Goldschmidt-Clermont, P.J.** (1997). Mitogenic signaling mediated by oxidants in Ras-
1061 transformed fibroblasts. Science **275,** 1649-1652.
1062 **Jank, T., Bogdanović, X., Wirth, C., Haaf, E., Spoerner, M., Böhmer, K.E., Steinemann, M., Orth, J.H.C.,**
1063 **Kalbitzer, H.R., Warscheid, B., Hunte, C., and Aktories, K.** (2013). A bacterial toxin catalyzing
1064 tyrosine glycosylation of Rho and deamidation of Gq and Gi proteins. Nature Structural &
1065 Molecular Biology **20,** 1273-1280.
1066 **Jones, M.A., Shen, J.-J., Fu, Y., Li, H., Yang, Z., and Grierson, C.S.** (2002). The Arabidopsis Rop2 GTPase
1067 is a positive regulator of both root hair initiation and tip growth. The Plant Cell **14,** 763-776.
1068 **Jurca, M.E., Bottka, S., and Fehér, A.** (2008). Characterization of a family of Arabidopsis receptor-like
1069 cytoplasmic kinases (RLCK class VI). Plant Cell Reports **27,** 739-748.
1070 **Katoh, K., and Toh, H.** (2010). Parallelization of the MAFFT multiple sequence alignment program.
1071 Bioinformatics **26,** 1899-1900.
1072 **Klahre, U., and Kost, B.** (2006). Tobacco RhoGTPase ACTIVATING PROTEIN1 Spatially Restricts Signaling
1073 of RAC/Rop to the Apex of Pollen Tubes. The Plant Cell **18,** 3033-3046.
1074 **Krauthammer, M., Kong, Y., Ha, B.H., Evans, P., Bacchiocchi, A., McCusker, J.P., Cheng, E., Davis, M.J.,**
1075 **Goh, G., Choi, M., Ariyan, S., Narayan, D., Dutton-Regester, K., Capatana, A., Holman, E.C.,**
1076 **Bosenberg, M., Sznol, M., Kluger, H.M., Brash, D.E., Stern, D.F., Materin, M.A., Lo, R.S.,**
1077 **Mane, S., Ma, S., Kidd, K.K., Hayward, N.K., Lifton, R.P., Schlessinger, J., Boggon, T.J., and**
1078 **Halaban, R.** (2012). Exome sequencing identifies recurrent somatic RAC1 mutations in
1079 melanoma. Nat Genet **44,** 1006-1014.
1080 **Lang, P., Gesbert, F., Delespine-Carmagnat, M., Stancou, R., Pouchelet, M., and Bertoglio, J.** (1996).
1081 Protein kinase A phosphorylation of RhoA mediates the morphological and functional effects
1082 of cyclic AMP in cytotoxic lymphocytes. EMBO J **15,** 510-519.
1083 **Lawson, C.D., and Ridley, A.J.** (2018). Rho GTPase signaling complexes in cell migration and invasion.
1084 J Cell Biol **217,** 447-457.
1085 **Lazo, G.R., Stein, P.A., and Ludwig, R.A.** (1991). A DNA transformation-competent Arabidopsis
1086 genomic library in Agrobacterium. Biotechnology (N Y) **9,** 963-967.
1087 **Lin, Y., and Yang, Z.** (1997). Inhibition of Pollen Tube Elongation by Microinjected Anti-Rop1Ps
1088 Antibodies Suggests a Crucial Role for Rho-Type GTPases in the Control of Tip Growth. Plant
1089 Cell **9,** 1647-1659.

1090 **Lu, D., Lin, W., Gao, X., Wu, S., Cheng, C., Avila, J., Heese, A., Devarenne, T.P., He, P., and Shan, L.**
1091 (2011). Direct ubiquitination of pattern recognition receptor FLS2 attenuates plant innate
1092 immunity. Science **332,** 1439-1442.
1093 **MacLean, B., Tomazela, D.M., Shulman, N., Chambers, M., Finney, G.L., Frewen, B., Kern, R., Tabb,**
1094 **D.L., Liebler, D.C., and MacCoss, M.J.** (2010). Skyline: an open source document editor for
1095 creating and analyzing targeted proteomics experiments. Bioinformatics **26,** 966-968.
1096 **Marx, H., Lemeer, S., Schliep, J.E., Matheron, L., Mohammed, S., Cox, J., Mann, M., Heck, A.J., and**
1097 **Kuster, B.** (2013). A large synthetic peptide and phosphopeptide reference library for mass
1098 spectrometry–based proteomics. Nature biotechnology **31,** 557-564.
1099 **McCollum, C., Engelhardt, S., Weiss, L., and Hückelhoven, R.** (2020). ROP INTERACTIVE PARTNER b
1100 Interacts with RACB and Supports Fungal Penetration into Barley Epidermal Cells. Plant
1101 Physiology **184,** 823-836.
1102 **Mergner, J., Frejno, M., List, M., Papacek, M., Chen, X., Chaudhary, A., Samaras, P., Richter, S.,**
1103 **Shikata, H., Messerer, M., Lang, D., Altmann, S., Cyprys, P., Zolg, D.P., Mathieson, T.,**
1104 **Bantscheff, M., Hazarika, R.R., Schmidt, T., Dawid, C., Dunkel, A., Hofmann, T., Sprunck, S.,**
1105 **Falter-Braun, P., Johannes, F., Mayer, K.F.X., Jürgens, G., Wilhelm, M., Baumbach, J., Grill, E.,**
1106 **Schneitz, K., Schwechheimer, C., and Kuster, B.** (2020). Mass-spectrometry-based draft of the
1107 Arabidopsis proteome. Nature.
1108 **Milburn, M.V., Tong, L., deVos, A.M., Brunger, A., Yamaizumi, Z., Nishimura, S., and Kim, S.H.** (1990).
1109 Molecular switch for signal transduction: structural differences between active and inactive
1110 forms of protooncogenic ras proteins. Science **247,** 939.
1111 **Oberoi, T.K., Dogan, T., Hocking, J.C., Scholz, R.-P., Mooz, J., Anderson, C.L., Karreman, C., Meyer zu**
1112 **Heringdorf, D., Schmidt, G., Ruonala, M., Namikawa, K., Harms, G.S., Carpy, A., Macek, B.,**
1113 **Köster, R.W., and Rajalingam, K.** (2012). IAPs regulate the plasticity of cell migration by
1114 directly targeting Rac1 for degradation. The EMBO journal **31,** 14-28.
1115 **Opalski, K.S., Schultheiss, H., Kogel, K.H., and Huckelhoven, R.** (2005). The receptor-like MLO protein
1116 and the RAC/ROP family G-protein RACB modulate actin reorganization in barley attacked by
1117 the biotrophic powdery mildew fungus Blumeria graminis f.sp. hordei. Plant J **41,** 291-303.
1118 **Ozdamar, B., Bose, R., Barrios-Rodiles, M., Wang, H.R., Zhang, Y., and Wrana, J.L.** (2005). Regulation
1119 of the polarity protein Par6 by TGFbeta receptors controls epithelial cell plasticity. Science **307,**
1120 1603-1609.
1121 **Pai, E.F., Kabsch, W., Krengel, U., Holmes, K.C., John, J., and Wittinghofer, A.** (1989). Structure of the
1122 guanine-nucleotide-binding domain of the Ha-ras oncogene product p21 in the triphosphate
1123 conformation. Nature **341,** 209-214.
1124 **Pathuri, I.P., Zellerhoff, N., Schaffrath, U., Hensel, G., Kumlehn, J., Kogel, K.H., Eichmann, R., and**
1125 **Huckelhoven, R.** (2008). Constitutively activated barley ROPs modulate epidermal cell size,
1126 defense reactions and interactions with fungal leaf pathogens. Plant Cell Rep **27,** 1877-1887.
1127 **Peng, J., Schwartz, D., Elias, J.E., Thoreen, C.C., Cheng, D., Marsischky, G., Roelofs, J., Finley, D., and**
1128 **Gygi, S.P.** (2003). A proteomics approach to understanding protein ubiquitination. Nat
1129 Biotechnol **21,** 921-926.
1130 **Rademacher, E.H., and Offringa, R.** (2012). Evolutionary Adaptations of Plant AGC Kinases: From Light
1131 Signaling to Cell Polarity Regulation. Front Plant Sci **3,** 250.
1132 **Reiner, T., Hoefle, C., and Hückelhoven, R.** (2016). A barley SKP1-like protein controls abundance of
1133 the susceptibility factor RACB and influences the interaction of barley with the barley powdery
1134 mildew fungus. Molecular plant pathology **17,** 184-195.
1135 **Reiner, T., Hoefle, C., Huesmann, C., Ménesi, D., Fehér, A., and Hückelhoven, R.** (2015). The
1136 Arabidopsis ROP-activated receptor-like cytoplasmic kinase RLCK VI_A3 is involved in control
1137 of basal resistance to powdery mildew and trichome branching. Plant Cell Reports **34,** 457-
1138 468.
1139 **Rolli-Derkinderen, M., Sauzeau, V., Boyer, L., Lemichez, E., Baron, C., Henrion, D., Loirand, G., and**
1140 **Pacaud, P.** (2005). Phosphorylation of serine 188 protects RhoA from ubiquitin/proteasome-
1141 mediated degradation in vascular smooth muscle cells. Circ Res **96,** 1152-1160.

1142 **Ruprecht, B., Zecha, J., Zolg, D.P., and Kuster, B.** (2017a). High pH Reversed-Phase Micro-Columns for
1143 Simple, Sensitive, and Efficient Fractionation of Proteome and (TMT labeled)
1144 Phosphoproteome Digests. Methods Mol Biol **1550,** 83-98.
1145 **Ruprecht, B., Koch, H., Domasinska, P., Frejno, M., Kuster, B., and Lemeer, S.** (2017b). Optimized
1146 Enrichment of Phosphoproteomes by Fe-IMAC Column Chromatography. Methods Mol Biol
1147 **1550,** 47-60.
1148 **Schaefer, A., Höhner, K., Berken, A., and Wittinghofer, A.** (2011). The unique plant RhoGAPs are
1149 dimeric and contain a CRIB motif required for affinity and specificity towards cognate small G
1150 proteins. Biopolymers **95,** 420-433.
1151 **Schindelin, J., Arganda-Carreras, I., Frise, E., Kaynig, V., Longair, M., Pietzsch, T., Preibisch, S.,**
1152 **Rueden, C., Saalfeld, S., and Schmid, B.** (2012). Fiji: an open-source platform for biological-
1153 image analysis. Nature methods **9,** 676-682.
1154 **Schrodinger, LLC.** (2015). The PyMOL Molecular Graphics System, Version 1.8.
1155 **Schultheiss, H., Dechert, C., Kogel, K.-H., and Hückelhoven, R.** (2002). A small GTP-binding host
1156 protein is required for entry of powdery mildew fungus into epidermal cells of barley. Plant
1157 Physiology **128,** 1447-1454.
1158 **Schultheiss, H., Dechert, C., Kogel, K.H., and Huckelhoven, R.** (2003). Functional analysis of barley
1159 RAC/ROP G-protein family members in susceptibility to the powdery mildew fungus. Plant J
1160 **36,** 589-601.
1161 **Schultheiss, H., Preuss, J., Pircher, T., Eichmann, R., and Huckelhoven, R.** (2008). Barley RIC171
1162 interacts with RACB in planta and supports entry of the powdery mildew fungus. Cell Microbiol
1163 **10,** 1815-1826.
1164 **Schweizer, P., Pokorny, J., Abderhalden, O., and Dudler, R.** (1999). A Transient Assay System for the
1165 Functional Assessment of Defense-Related Genes in Wheat. Molecular Plant-Microbe
1166 Interactions **12,** 647-654.
1167 **Sorek, N., Poraty, L., Sternberg, H., Buriakovsky, E., Bar, E., Lewinsohn, E., and Yalovsky, S.** (2017).
1168 Corrected and Republished from: Activation Status-Coupled Transient S-Acylation Determines
1169 Membrane Partitioning of a Plant Rho-Related GTPase. Molecular and Cellular Biology **37,**
1170 e00333-00317.
1171 **Sorek, N., Segev, O., Gutman, O., Bar, E., Richter, S., Poraty, L., Hirsch, J.A., Henis, Y.I., Lewinsohn, E.,**
1172 **Jürgens, G., and Yalovsky, S.** (2010). An S-Acylation Switch of Conserved G Domain Cysteines
1173 Is Required for Polarity Signaling by ROP GTPases. Current Biology **20,** 914-920.
1174 **Sorek, N., Gutman, O., Bar, E., Abu-Abied, M., Feng, X., Running, M.P., Lewinsohn, E., Ori, N., Sadot,**
1175 **E., Henis, Y.I., and Yalovsky, S.** (2011). Differential effects of prenylation and s-acylation on
1176 type I and II ROPS membrane interaction and function. Plant Physiol **155,** 706-720.
1177 **Sørmo, C.G., Leiros, I., Brembu, T., Winge, P., Os, V., and Bones, A.M.** (2006). The crystal structure of
1178 Arabidopsis thaliana RAC7/ROP9: the first RAS superfamily GTPase from the plant kingdom.
1179 Phytochemistry **67,** 2332-2340.
1180 **Stanislas, T., Huser, A., Barbosa, I.C., Kiefer, C.S., Brackmann, K., Pietra, S., Gustavsson, A.,**
1181 **Zourelidou, M., Schwechheimer, C., and Grebe, M.** (2015). Arabidopsis D6PK is a lipid domain-
1182 dependent mediator of root epidermal planar polarity. Nat Plants **1,** 15162.
1183 **Studer, G., Rempfer, C., Waterhouse, A.M., Gumienny, R., Haas, J., and Schwede, T.** (2020).
1184 QMEANDisCo-distance constraints applied on model quality estimation. Bioinformatics **36,**
1185 1765-1771.
1186 **Tang, J., Ip, J.P.K., Ye, T., Ng, Y.-P., Yung, W.-H., Wu, Z., Fang, W., Fu, A.K.Y., and Ip, N.Y.** (2014). Cdk5-
1187 Dependent Mst3 Phosphorylation and Activity Regulate Neuronal Migration through RhoA
1188 Inhibition. The Journal of Neuroscience **34,** 7425-7436.
1189 **Thomas, C., Fricke, I., Scrima, A., Berken, A., and Wittinghofer, A.** (2007). Structural evidence for a
1190 common intermediate in small G protein-GEF reactions. Mol Cell **25,** 141-149.
1191 **Tong, J., Li, L., Ballermann, B., and Wang, Z.** (2016). Phosphorylation and Activation of RhoA by ERK in
1192 Response to Epidermal Growth Factor Stimulation. PLoS One **11,** e0147103.

1193 **Torrino, S., Visvikis, O., Doye, A., Boyer, L., Stefani, C., Munro, P., Bertoglio, J., Gacon, G., Mettouchi,**
1194 **A., and Lemichez, E.** (2011). The E3 ubiquitin-ligase HACE1 catalyzes the ubiquitylation of
1195 active Rac1. Dev Cell **21,** 959-965.
1196 **Vickers, C.E., Xue, G.P., and Gresshoff, P.M.** (2003). A synthetic xylanase as a novel reporter in plants.
1197 Plant Cell Reports **22,** 135-140.
1198 **Vizcaíno, J.A., Csordas, A., Del-Toro, N., Dianes, J.A., Griss, J., Lavidas, I., Mayer, G., Perez-Riverol, Y.,**
1199 **Reisinger, F., and Ternent, T.** (2016). 2016 update of the PRIDE database and its related tools.
1200 Nucleic acids research **44,** D447-D456.
1201 **Wang, H.-R., Zhang, Y., Ozdamar, B., Ogunjimi, A.A., Alexandrova, E., Thomsen, G.H., and Wrana, J.L.**
1202 (2003). Regulation of Cell Polarity and Protrusion Formation by Targeting RhoA for
1203 Degradation. Science **302,** 1775-1779.
1204 **Waterhouse, A., Bertoni, M., Bienert, S., Studer, G., Tauriello, G., Gumienny, R., Heer, F.T., de Beer,**
1205 **T.A.P., Rempfer, C., and Bordoli, L.** (2018). SWISS-MODEL: homology modelling of protein
1206 structures and complexes. Nucleic acids research **46,** W296-W303.
1207 **Waterhouse, A.M., Procter, J.B., Martin, D.M., Clamp, M., and Barton, G.J.** (2009). Jalview Version 2-
1208 -a multiple sequence alignment editor and analysis workbench. Bioinformatics **25,** 1189-1191.
1209 **Wei, J., Mialki, R.K., Dong, S., Khoo, A., Mallampalli, R.K., Zhao, Y., and Zhao, J.** (2013). A new
1210 mechanism of RhoA ubiquitination and degradation: roles of SCF(FBXL19) E3 ligase and Erk2.
1211 Biochim Biophys Acta **1833,** 2757-2764.
1212 **Wennerberg, K., Rossman, K.L., and Der, C.J.** (2005). The Ras superfamily at a glance. J Cell Sci **118,**
1213 843-846.
1214 **Worby, C.A., Mattoo, S., Kruger, R.P., Corbeil, L.B., Koller, A., Mendez, J.C., Zekarias, B., Lazar, C., and**
1215 **Dixon, J.E.** (2009). The fic domain: regulation of cell signaling by adenylylation. Mol Cell **34,** 93-
1216 103.
1217 **Wu, G., Li, H., and Yang, Z.** (2000). Arabidopsis RopGAPs Are a Novel Family of Rho GTPase-Activating
1218 Proteins that Require the Cdc42/Rac-Interactive Binding Motif for Rop-Specific GTPase
1219 Stimulation. Plant Physiology **124,** 1625-1636.
1220 **Yalovsky, S.** (2015). Protein lipid modifications and the regulation of ROP GTPase function. J Exp Bot
1221 **66,** 1617-1624.
1222 **Yang, Z.** (2008). Cell polarity signaling in Arabidopsis. Annu Rev Cell Dev Biol **24,** 551-575.
1223 **Zhao, J., Mialki, R.K., Wei, J., Coon, T.A., Zou, C., Chen, B.B., Mallampalli, R.K., and Zhao, Y.** (2013).
1224 SCF E3 ligase F-box protein complex SCFFBXL19 regulates cell migration by mediating Rac1
1225 ubiquitination and degradation. The FASEB Journal **27,** 2611-2619.
1226 **Zolg, D.P., Wilhelm, M., Yu, P., Knaute, T., Zerweck, J., Wenschuh, H., Reimer, U., Schnatbaum, K.,**
1227 **and Kuster, B.** (2017). PROCAL: A Set of 40 Peptide Standards for Retention Time Indexing,
1228 Column Performance Monitoring, and Collision Energy Calibration. PROTEOMICS **17,** 1700263.
1229 **Zolg, D.P., Wilhelm, M., Schmidt, T., Medard, G., Zerweck, J., Knaute, T., Wenschuh, H., Reimer, U.,**
1230 **Schnatbaum, K., and Kuster, B.** (2018). ProteomeTools: Systematic characterization of 21
1231 post-translational protein modifications by liquid chromatography tandem mass spectrometry
1232 (LC-MS/MS) using synthetic peptides. Molecular & Cellular Proteomics **17,** 1850-1863.

1233

1234

Supporting information

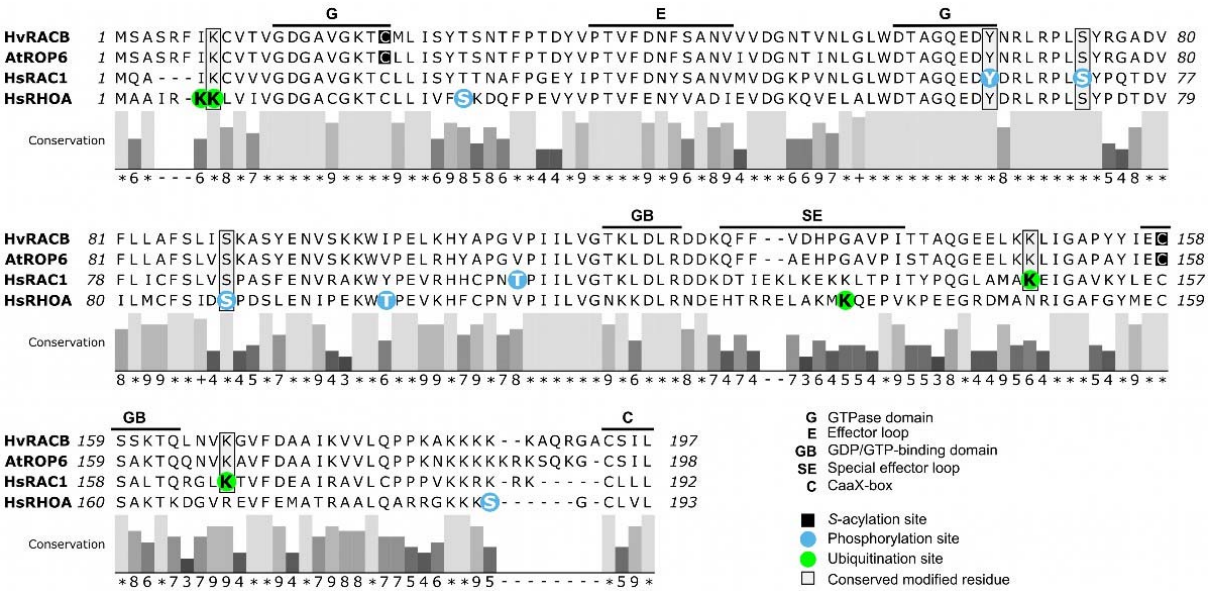

S1 Fig. Alignment of RACB with AtROP6, HsRAC1 and HsRHOA.

Previously published phosphorylation (blue) and ubiquitination (green) sites of mammalian Rac1 and RhoA are highlighted here in the human RAC1 and RHOA sequences. Conserved sites are highlighted in grey boxes. Additionally, the GTPase domain (G), effector loop (E), nucleotide-binding domain (GB), special effector loop (SE) and CaaX-box prenylation motif (C) are illustrated and were taken from Schultheiss et al. (2003). AtROP6 has been shown to be transiently *S*-acylated at two cysteines (Sorek et al., 2010; Sorek et al., 2017), which are also conserved in RACB (black boxes). Conservation of amino acids was determined using MAFFT multiple-sequence alignment in Jalview (Waterhouse et al., 2009; Katoh and Toh, 2010). Conservation scores range from 0 to 11 and are shown as bars (dark grey = less conserved, light grey = highly conserved). Scores of 0, 10, and 11 are shown as “-“, “+” and “*”, respectively).

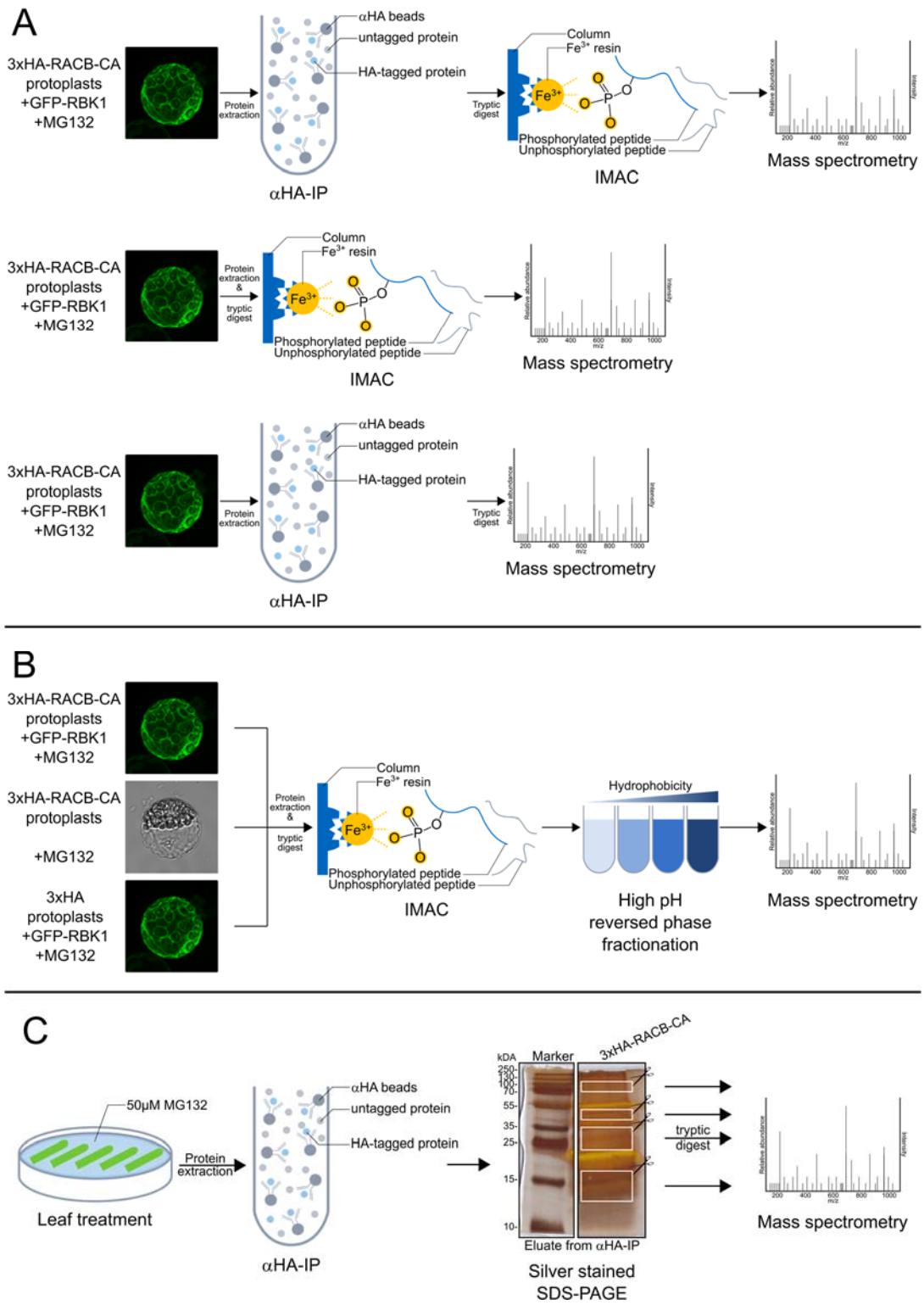

1252

1253 **S2 Fig. Workflows designed to identify RACB phosphorylation and ubiquitination.**

1254 **(A)** Identification of phosphorylated peptides after CA-RACB and RBK1 overexpression.
1255 Protoplasts were isolated from stably-transgenic barley leaves overexpressing 3xHA-CA-
1256 RACB (pooled lines BG657 E3 and E4). These protoplasts were transiently super-transformed

1257 with GFP-RBK1 to stimulate phosphorylation events of proteins associated with the
1258 RACB/RBK1 pathway. After transformation, all protoplasts were treated with MG132 and
1259 proteins were extracted. HA-tagged proteins were first enriched using immunoprecipitation,
1260 followed by tryptic digest and phosphopeptide enrichment via IMAC (top panel). In two cases,
1261 immunoprecipitation or IMAC were skipped (center and lower panel, respectively).
1262 Phosphorylated peptides were identified using mass spectrometry.

1263 **(B)** Second experiment to identify phosphorylated peptides after CA-RACB and/or RBK1
1264 overexpression. Protoplasts were isolated from stably transgenic barley leaves overexpressing
1265 either 3xHA (lines BG659 E2 and E3) or 3xHA-CA-RACB (lines BG657 E3 and E4). These
1266 protoplasts were super-transformed with GFP-RBK1. After transformation, all protoplasts
1267 (including an untransformed 3xHA-CA-RACB control) were treated with MG132. Proteins were
1268 extracted and digested with trypsin, followed by enrichment of phosphopeptides using IMAC.
1269 These samples were decomplexed by fractionating the phosphorylated proteins according to
1270 their hydrophobicity. Phosphorylated peptides were identified by mass spectrometry.

1271 **(C)** Analysis of CA-RACB ubiquitination by a targeted approach. Transgenic barley leaves
1272 overexpressing 3xHA-CA-RACB (from pooled lines BG657 E3 and E4) were floated on a
1273 solution containing MG132. HA-containing proteins were enriched by immunoprecipitation and
1274 loaded on a SDS-PAGE. Following silver-staining, RACB-containing bands and those
1275 corresponding to the higher molecular weight derivatives shown in Fig 5A were excised from
1276 the gel (white boxes). After solubilization and tryptic digest, modification of RACB-peptides
1277 was investigated via mass spectrometry.

1278

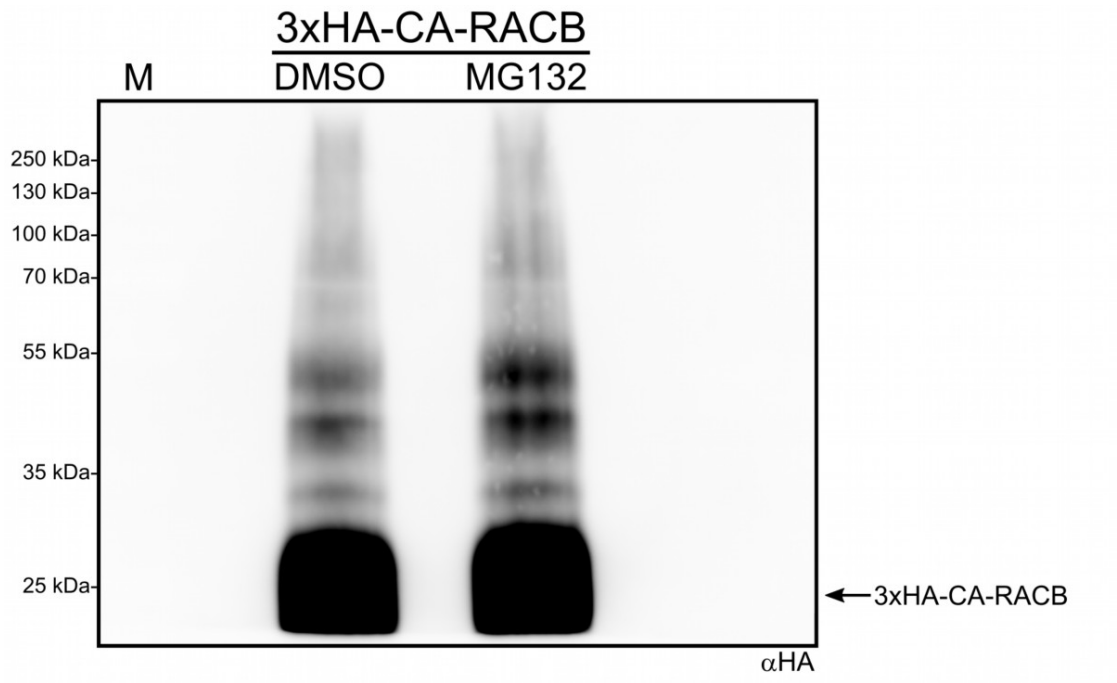

1279

1280

1281 **S3 Fig. The ubiquitin-like laddering pattern of 3xHA-CA-RACB is independent of MG132.**

1282 Whole first leaves of barley stably overexpressing 3xHA-CA-RACB were either floated on a
1283 solution containing MG132 or DMSO. After protein extraction, αHA-immunoprecipitation and
1284 αHA Western blotting, higher molecular weight laddering of 3xHA-CA-RACB could be detected
1285 independent of the treatment. Plant material originated from transgenic lines BG657 E3 and
1286 E4.

1287

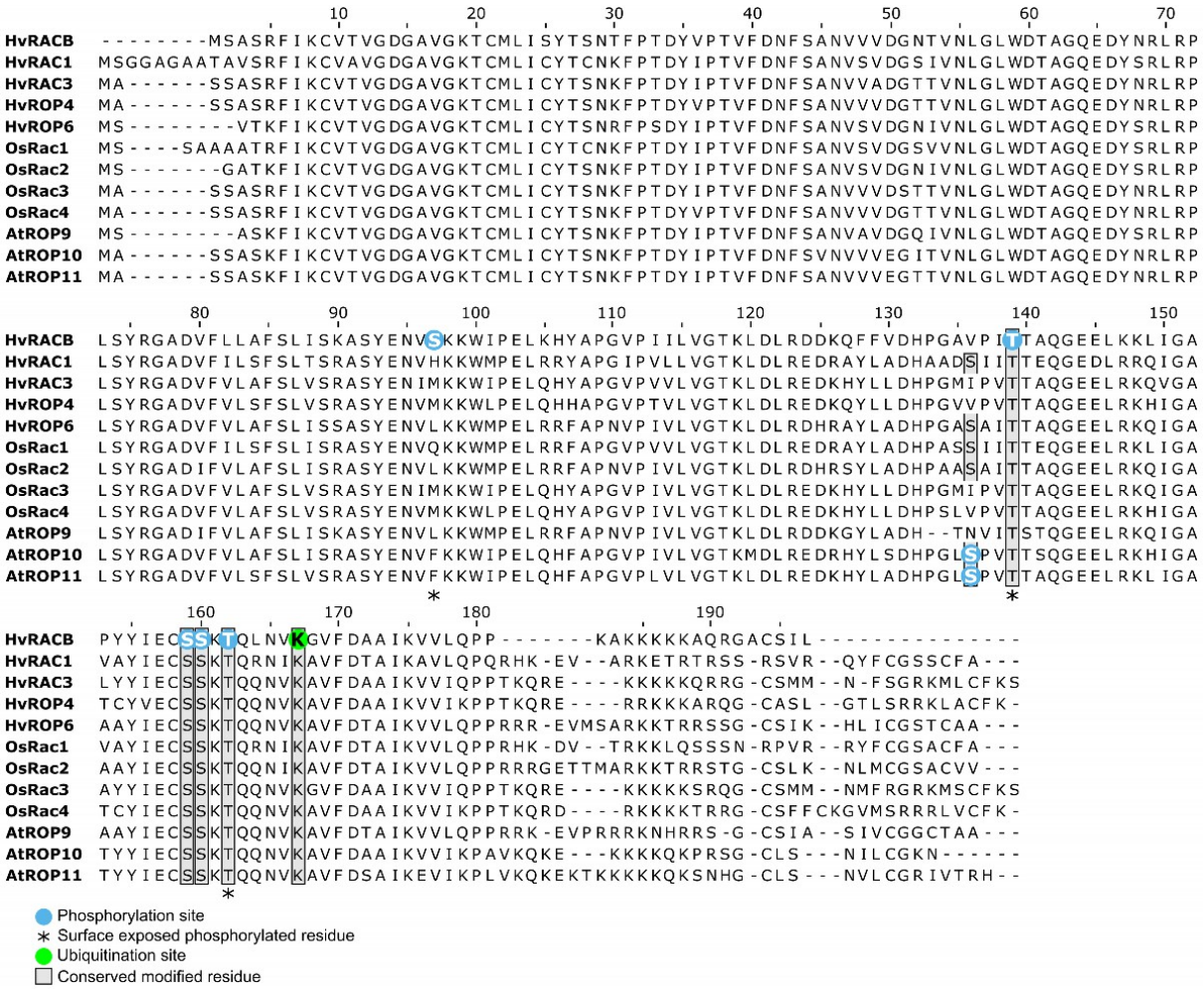

S4 Fig. Alignment of barley RACB with type II ROPs from barley, rice *Arabidopsis thaliana*.

The CA-RACB ubiquitination site at K167 (green) is conserved in all type II ROPs from the three species (shaded box). *In vitro* phosphorylation sites of RACB (blue) are conserved among most type II ROPs (shaded box). Surface-exposed phosphosites are indicated by asterisks. Conserved amino acids were identified and aligned using MAFFT multiple-sequence alignment in Jalview (Waterhouse et al., 2009; Katoh and Toh, 2010).

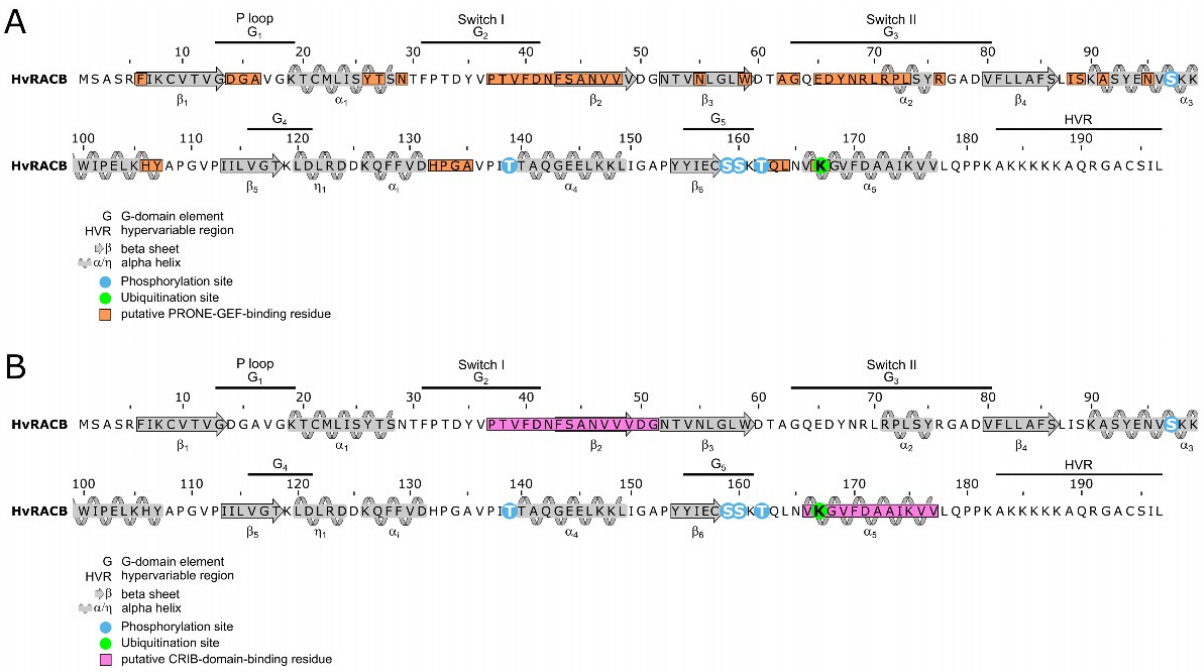

S5 Fig. GEF- and CRIB-binding interfaces in RACB.

Predicted binding interfaces for PRONE-GEFs (**A**, orange boxes, (Thomas et al., 2007)) and CRIB-domains (**B**, pink boxes, (Abdul-Manan et al., 1999; Schaefer et al., 2011)) are highlighted in the RACB amino acid sequence. RACB secondary structure motifs were obtained through homology-modelling using SWISS-MODEL with the crystal structure of AtROP5 as template (PDB: 3bwd.1, (Fricke and Berken, 2009)). α-helices (grey boxes with winding helices) and β-sheets (grey arrows), as well as RACB *in vitro* phosphorylation (blue circle) and *in vivo* ubiquitination (green circle) sites are illustrated. Annotations for the G-domains (G_{1-5}) and hypervariable region (HVR) were taken from Fricke and Berken (2009), whereas regions for P loop and Switches I & II were adopted from Sørmo et al. (2006). Numbering for α-helices and β-sheets follow Pai et al. (1989) and Thomas et al. (2007).

1311 **S1 Table. Dataset of the mass spectrometry analysis of the recombinant RACB and**
1312 **RBK1 *in vitro* kinase assay.**

1313 **S2 Table. Dataset of the first mass-spectrometry experiment to identify *in vivo***
1314 **phosphorylation of CA-RACB.** This dataset contains all identified barley phosphopeptides
1315 originating from transgenic HA-CA-RACB overexpressing protoplasts, which were transformed
1316 with GFP-RBK1 and treated with MG132. HA-tagged proteins and/or phosphopeptides were
1317 enriched by HA-immunoprecipitation and IMAC, respectively (S2A Fig). All peptides and their
1318 modifications were identified by mass spectrometry. Of main interest are the gene identifiers
1319 and peptides with phosphorylated residues and associated localization scores.

1320 **S3 Table. Dataset of the second mass-spectrometry experiment to identify *in vivo***
1321 **phosphorylation of CA-RACB.** Dataset comprising all recovered barley phosphopeptides
1322 from protoplasts of stable transgenic barley plants. Phosphopeptides were enriched from
1323 full-protein extracts of either HA- or HA-CA-RACB overexpressing protoplasts, which were co-
1324 transformed with GFP-RBK1 and incubated with MG132. Samples were decomplexed by
1325 fractionating phosphopeptides according to their hydrophobicity (S2B Fig). All peptides and
1326 their modifications were identified by mass spectrometry. Non-enriched full-protein samples
1327 (FP) were included in mass spectrometry analyses, but did not yield many phosphopeptides.
1328 Of main interest in this dataset are the gene identifiers and peptides with phosphorylated amino
1329 acids and their corresponding localization scores.

1330 **S4 Table. Summary of all barley ROPGAP phosphorylation sites which were evidenced**
1331 **in this study.**

1332 **S5 Table. List of all primers used in this study.**

1333